DAFTAR PUSTAKA

Alloway, B. J & Ayres, D. C.,1997. *Chemical Principles of Environmental Pollution.* Blackie Academic & Professional (Chapman & Hall): 205-211.

Almughamisi, M. S., Khan, Z. A., Alshitari, W., & Elwakeel, K. Z., 2020. Recovery of Chromium(VI) Oxyanions from Aqueous Solution using $Cu(OH)_2$ and CuO Embedded Chitosan Adsorbents. *Journal of Polymers and the Environment* **28**(3): 1-14.

Aziz, N. A. A., & Jalil, A.M.M., 2019. Potential Health Benefits of Indigenous Durian (*Durio zibethinus* Murr.). A Review. *Foods,* **8**(3): 96.

Badan Pusat Statistik, 2020. *Produksi Tanaman Buah-buahan 2020 di Indonesia.(online:* https://www.bps.go.id/indicator/55/62/1/produksi-tanaman-buah-buahan.html (diakses 14 maret 2021).

Baig, U., Rao, R. A. K., Khan, A. A., Sanagi, M. M.,. Gondal, M. A., 2015. Removal of Carcinogenic Hexavalent Chromium from Aqueous Solutions Using Newly Synthesized and Characterized Polypyrrole-Titanium(IV) Phosphate Nanocomposite, *Chemical Engineering Journal*, **280**(2015): 494-504.

Beltramino, F., Roncero, M.B., Torres, A.L., Vidal, T., & Valls, C., 2016. Optimization of Sulfuric Acid Hydrolysis Conditions for Preparation of Nanocrystalline Cellulose from Enzymatically Pretreated Fibers. *Cellulos.*, **23**: 1777-1789.

Bidgoli, H., Mortazavi, Y., Khodadadi, A. A., 2019. A functionalized nano-structured cellulosic sorbent aerogel for oil spill cleanup: synthesis and characterization. *Journal of Hazardous Materials*, **366**: 229-239.

Brady, J.E., & Humiston, 1999. *General Chemistry Principle and Structure, 4 th edition*. New York: John Willey & Sons, Inc.

Callister, Jr William D., 2009. *Materials Science and Engineering An Introduction, 8th Edition*. New Jersey: John Wiley & Sons, Inc, Hoboken.

Cervin, N.T., Aulin, C., Larsson, P. T., & Wagberg, L., 2012. Ultra Porous Nanocellulose Aero-Gels as Separation Medium for Mixtures of Oil/Water Liquids. *Cellulose*, **19:** 401-410.

Ciolacu, D., Ciolacu, F., & Popa, V. I., 2011. Amorphous Cellulose-Structure and Characterization. *Cellulose Chemistry Technology*. **45**(1-2): 13-2.

Danish, M., Tanweer, A., Shahnaz, M., Mehraj, A., Lou, Z., Zhou Pin, & S. M. S. Iqubal, 2018. Use of Banana Trunk Waste as Activated Carbon in Scavenging Methylene Blue Dye: Kinetic, Thermodynamic, and Isotherm Studies. *Bioresource Technology*, **3**(4): 127-137.

Defrance, K. J., Hoare, T., & Cranston, E. D., 2017. Review of Hydrogels and Aerogels Containing Nanocellulose. Chemistry of Materials, **29**(11): 4609-4631.

DesMarais, T. L., & Costa, M., 2019. Mechanisms of Chromium-Induced Toxicity. *Current Opinion in Toxicology.*

Dilamian, M., & Noroozi, B., 2021. Rice straw agri-waste for water pollutant adsorption: Relevant mesoporous super hydrophobic cellulose aerogel. *Carbohydrate Polymers.* **251**(2020): 117016.

Fardiaz S., 1992. *Polusi Air dan Udara*. Yogyakarta: Kasinius.

Feng, J., Wang, Y., Yi, X., Yang, W., & He, X., 2016. Phenolics from Durian Exert Pronounced NO Inhibitory and Antioxidant Activities. *Journal of Agricultural and Food Chemistry,* **64**(21): 4273-4279.

Fengel, D. & G. Wegener, 1995. *Kayu: Kimia, Ultrastuktur, Reaksi-reaksi*, Diterjemahkan oleh Hardjono Sastrohamidjojo. Yogyakarta: Gadjah Mada University Press.

Fernando, V. A. K., Weerasena, J., Lakraj, G. P., Perera, I. C., Dangalle, C. D., Handunnetti, S., & Wijesinghe, M. R., 2016. Lethal and Sub-Lethal Effects on The Asian Common Toad Duttaphrynus Melanostictus from Exposure to Hexavalent Chromium. *Aquatic Toxicology,* **177**: 98-105.

Fricke, J., & Emmerling, A., 1992. Aerogels. *Journal of the American Ceramic Society*, **75**(8): 2027-2035.

Fu, X., Ji, H., Wang, B., Zhu, W., Pang, Z., & Dong, C., 2020. Preparation of Thermally Stable and Surface-Functionalized Cellulose Nanocrystals by a Fully Recyclable Organic Acid and Ionic Liquid Mediated Technique Under Mild Conditions. *Cellulose*, **27**: 1289-1299.

Fuller, M.E., Andaya, C., & McClay, K., 2018. Evaluation of ATR-FTIR for Analysis of Bacterial Cellulose Impurities, *Journal of Microbiological Methods*, **144**: 145-151.

Ganguly, P., Sengupta, S., Das, P., & Bhowal, A. (2020). Valorization of food waste: Extraction of cellulose, lignin and their application in energy use and water treatment. *Fuel,* **280**(6): 118581.

Gustinenda, Beta Y., & Margo, K. C., 2017. Sintesis Superabsorben Aerogel Selulosa berbasis Sabut Kelapa. Institut Teknologi Sepuluh Nopember.

Haafiz, M.M., Eichhorn, S., Hassan, A., & Jawaid, M., 2013., Isolation and Characterization of Microcrystalline Cellulose from Oil Palm Biomass Residue, Carbohydr. *Polym*, **93** (2): 628-634.

Hayes, W. A. & Kruger. C. L., 2014. *Hayes Priciple And Methods Of Toxicology Sictd Edition.* New York: Taylor & Francis Grup.

He, Q., Wang, Q., Zhou, H., Ren, D., He, Y., Cong, H., & Wu, L., 2018. Highly Crystalline Cellulose from Brown Seaweed Saccharina Japonica: Isolation, Characterization and Microcrystallization. *Cellulose.* **25**, 5523-5533.

Hosseini, H., & Mousavi, S. M., 2020. Bacterial Cellulose/polyaniline Nanocomposite Aerogels as Novel Bioadsorbents for Removal of Hexavalent Chromium: Experimental and simulation study. *Journal of Cleaner Production*, **278**: 123817.

Hou, W., Ling, C., Shi, S., & Yan, Z., 2019. Preparation and Characterization of Microcrystalline Cellulose from Waste Cotton Fabrics by using Phosphotungstic Acid, *Int. J. Biol. Macromol*, **123**: 363-368

Huheey, J. E., Keiter, E. A., & Keiter, R., 1997. *Inorganic Chemistry: Principles of Structure and Reactivity,* 4th ed. New York: Harper Collins.

Kargarzadeh, H., Mariano, M., Huang, J., Lin, N., Ahmad, I., Dufresne, A., & Thomas, S. 2017. Recent Developments on Nanocellulose Reinforced Polymer Nanocomposites: A review. *Polymer,* **132**: 368-393.

Kaya, M. & Tabak, A., 2020. Recycling of an Agricultural Bio-waste as a Novel Cellulose Aerogel: A Green Chemistry Study. *Journal of Polymers and the Environment*, **8**(1): 323-330.

Kolanski, K.W., 2002. *Surface Science: Foundation of catalysis and Nano Science.* Inggris: John wiley and Sons Ltd.

Korhonen, J. T., Kettunen, M., Ras, R. H. A., & Ikkala, O., 2011. Hydrophobic Nanocellulose Aerogels as Floating, Sustainable, Reusable, and Recyclable Oil Absorbents*. ACS Applied Materials & Interfaces,* **3**(6): 1813-1816.

Kumar, A., Y. S. Negi, V.Choudhary & N. K.Bhardwaj. 2014. Characterization of Cellulose Nanocrystals Produced by Acid-Hydrolysis from Sugarcane Bagasse as Agro-Waste. *Journal of Materials Physics and Chemistry*, **2**(1): 1-8.

Kunusa, W. R., 2017. Kajian Tentang Isolasi Selulosa Mikrokristalin (SM) dari Limbah Tongkol Jagung*. Jurnal Entropi*, **12**(1): 105-108.

Lehninger, 2008. *Dasar-dasar biokimia Jilid 1 (Principles of Biochemistry).* Terj. Maggy Thenawijaya*.* Jakarta: Erlangga.

Li, D., Tian, X., Wang, Z., Guan, Z., Li, X., Qiao, H., & Wei, Q. 2019. Multifunctional Adsorbent Based on Metal-Organic Framework Modified Bacterial Cellulose/Chitosan Composite Aerogel for High Efficient Removal of Heavy Metal Ion and Organic Pollutant*. Chemical Engineering Journal,* **383**: 123127*.*

Li, N., Yue, Q., Gao, B., Xu, X., Kan, Y., & Zhao, P. 2018. Magnetic Graphene Oxide Functionalized by Poly Dimethyl Diallyl Ammonium Chloride for Efficient Removal of Cr(VI*). J. Taiwan Inst. Chem. Eng,* **91**: 449-506.

Liang, L., Zhang, S., Goenaga, G. A., Meng, X., Zawodzinski T. A., & Ragauskas A. J., 2020. Chemically Cross-Linked Cellulose Nanocrystal Aerogels for Effective Removal of Cation Dye. *Frontiers in Chemistry*, **8**(7): 1-9.

Litschauer, M., Neouze A M.,Haimer E., Henniges U., Potthast A., Rosenau T., & Liebner F., 2011. Silica Modified Cellulosic Aerogels. *Cellulose*, **18**(1): 143-149.

Liu, H., Li, P., Zhang, T., Zhu, Y., & Qiu, F. 2020. Fabrication of Recyclable Magnetic Double-Base Aerogel with Waste Bioresource Bagasse as The Source of Fiber for the Enhanced Removal of Chromium Ions from Aqueous Solution. *Food Bioproducts Processing,***119**: 257-267.

Long, L.-Y., Li, F.-F., Weng, Y.-X., & Wang, Y.-Z., 2019. Effects of Sodium Montmorillonite on the Preparation and Properties of Cellulose Aerogels. *Polymers*. **11**(3): 415.

Long, L.-Y., Weng, Y.-X., & Wang, Y.-Z., 2018. Cellulose Aerogels: Synthesis, Applications, and Prospects. *Polymers,* **10**(6): 623.

Lubis, R., Riyanto., Wirjosentono, B., Eddyanto, & Septevani, A. 2019. Extraction and Characterization of Cellulose Fiber of Durian Rinds from North Sumatera as The Raw Material for Textile Fiber. *J. Phys. Conf. Ser*., **1232** (1): 1-10.

Lubis, R., Wirjosentono, B., & Amanda, A. 2020. Preparation , Characterization and Antimicrobial Activity of Grafted Cellulose Fiber from Durian Rind Waste. *Colloids and Surfaces A*, **604**(6): 125311.

Manahan, S. E., 1992. *Environmental Chemistry*. 6 th Ed. USA: Lewis Publisher.

Massel, R. I., 1996. *Principle of Adsorption and Reaction in Solid Surface*. Kanada: John Wiley and Sons Ltd.

Matouq, M., Nina, J., Mohammed, Q., Muna, H., Maha, Q., & Al Syouf. 2015. The Adsorption Kinetics and Modeling for Heavy Metals *Removal* from Wastewater by Moringa pods. *Journal of Enviromental Chemical Engineering,* **3**: 775-784.

McCabe, W. L., J. C. Smith, & P. Harriott., 2005. *Unit Operations of Chemical Engineering. Edisi Ketujuh.* New York: McGraw-Hill, Inc.

Mehr, M. R., Fekri, M.H., Omidali, F., Eftekhari, N., & Adergani, B. A., 2019. Removal of Chromium (VI) from Wastewater by Palm Kernel Shell-based on a Green Method. *Journal of Chemical Health Risks,* **9**(1): 75-86.

Mosier, N., Wyman, C., Dale, B., Elander, R., Lee, Y.Y., Holtzapple, M. & Ladisch, M., 2005. Features of Promising Technologies for Pretreatment of Lignocellulosic Biomass. *Bioresource Technology*, **96**(6): 673-683.

Muley, P., D. & Dorin Boldor., 2017. Advances In Biomass Pretreatment And Cellulosic Bioethanol Productionusing Microwave Heatin. *Proceedings of SEEP, Slovenia.*

Nedal Y. Abu-Thabit, Ahmed A. J., Abbas s. H, Anwar U.H, Yunusa U., & Ayman A., 2020. Isolation and Characterization of Microcrystalline Cellulose from date Seeds (*Phoenix dactylifera L.). International Journal of Biological Macromolecules*, **155**: 730-739.

Nemoto, J., Saito, T,. & Isogai, A., 2015. Simple Freeze-Drying Procedure for Producing Nanocellulose Aerogel-Containing, High-Performance Air Filters, **7**(35):19809-19815.

Neolaka, Y.A.B., Supriyanto, G., Darmokoesoemo, H., Kusuma, H.S. 2018. Characterization, Kinetic, and Isotherm Data For Cr(VI) Removal from Aqueous Solution By Cr(VI)-Imprinted Poly(4-VP-Co-MMA). *Supported on Activated Indonesia (Ende-Flores) Natural Zeolite Structure Data Br*, **17**: 969-979.

Nguyen, S T, Feng J., Shao K. Ng, Wong J P.W, Tan V. B C., & Duong H. M., 2014. Advanced Thermal Insulation and Absorption Properties of Recycledcellulose Aerogels. *Colloids and Surfaces A: Physicochem. Eng. Aspects*, **445**: 128-136.

Nguyen, T. C., Xuan, T. N., Do Man, T. T., Vu, Q. T., Van H. N., Duy T. N., Minh T. D., Thi L. N., Thi N. L. Ly, & Tha, H., 2020. Adsorption Ability for Toxic Chromium (VI) Ions in Aqueous Solution of Some Modified Oyster Shell Types. *Bioinorganic Chemistry and Applications,* **2020**: 1-17.

Nomanbhay, S. M & Palanisamy, K., 2005. Removal of Heavy Metal From Industrial Wastewater Using Chitosan Coated Oil Palm Shell Charcoal. *Electronic Journal of Biotechnology*, **8**(1): 14-27.

Nugraheni, H. M., Tri A. M., & Lailatul B., 2018. Pemanfaatan Limbah Kulit Buah Durian Mentega sebagai *Carboxymethyl Cellulose* (CMC). *Prosiding Seminar Nasional Sains, Teknologi dan Analisis Ke-1.*

Nurjannah, N., R., Sudiarti, T., & Rahmidar, L., 2020. Sintesis dan Karakterisasi Selulosa Termetilasi sebagai Biokomposit Hidrogel. *Al-kimiya*, **7**(1): 19-27.

Omari, H., Dehbi, A., Lammini, A., & Abdallaoui, A., 2019. Study of the Phosphorus Adsorption on the Sediments. *Journal of Chemistry,* **2019**(1): 1-10.

Oscik, 1982. *Adsorption.* England: Ellis Horwood Ltd.

Ozcan, A.S., Erdem, B., & Ozcan A., 2005. Adsorpstion of Bcid blue 193 from Aqueous Solutions Onto BTMA-Bentonte. Colloid Surf. A: Physicochem. *Eng. Aspects*, **266**: 73-81.

Park, S., Baker, J.O., Himmel, M.E., Parilla, P.A., & Johnson D.K., 2010. Cellulose Crystallinity Index: Measurement Techniques and Their Impact on Interpreting Cellulase Performance. *Biotechnology for Biofuels,* **3**(10): 1-10.

Pei, R., Li, Q., Liu, J., Yang, G., Wu, Q., Wu, M., & Liu, M., 2020. Adsorption/Reduction Behaviors of Modified Cellulose Aerogels for the Removal of Low Content of Cr(VI). *Journal of Polymers and the Environment*, **28**(8): 2199-2210.

Penjumras, P., Rahman, R. B. A., Talib, R. A., & Abdan, K., 2014. Extraction and Characterization of Cellulose from Durian Rind. *Proceeding Agriculture and Agricultural Science Proceding,* **2**: 237-243.

Rafieian, F., M. Hosseini, M. Jonoobi and Q. L. Yu (2018). Development of hydrophobic nanocellulose-based aerogel via chemical vapor deposition for oil separation for water treatment. *Cellulose*, **25**(8): 4695-4710.

Rahman, Md., Lutfor, Jian., Wong Z., Sarjadi, M.S, Sabrina, S., Sazmal E. A., Kawi B., & Baba M., 2021. Heavy Metals Removal from Electroplating Wastewater by Waste Fiber-Based Poly(amidoxime) Ligand. *Water*, **13**(9): 1-20.

Razal, N. A. M., Sohaimi, R. M., Othman, R. N.Ira. R. Abdullah, N. Demon, S. Z. Ngah, J. L. Yunus, W. M. Z. Wan, Y., W. Mohd H. W. Salleh, E. M. Norizan, M. N. & Halim, N. A., 2022. Comparative Study on Extraction of Cellulose Fiber from Rice Straw Waste from Chemo-Mechanical and Pulping Method. *Polymers (Basel),* **14**(3): 387.

Ren, G., Wang, X., Huang, P., Zhong, B., Zhang, Z., Yang, L., & Yang, X., 2017. Chromium (VI) Adsorption from Wastewater Using Porous Magnetite Nanoparticles Prepared from Titanium Residue by A Novel Solid-Phase Reduction Method. *Science of The Total Environment*, **607**: 900-910.

Resti, K. D. S., & Utami, B. 2019. Effectiveness of Rice Husk and Bagasse Fly Ash as Adsorbent of Cr Metal on Batch System. *Jurnal Kimia dan Pendidikan Kimia,* **4**(2):1-13.

Riama, G., Austrin V., & Prasetyowati, 2012. Pengaruh H_2O_2, Konsentrasi NaOH dan Waktu terhadap Derajat Putih Pulp dari Mahkota Nanas. *Jurnal Teknik Kimia*, 1**8**(3): 25-34.

Robinson, T., 1995. *Kandungan Organik Tumbuhan Tinggi*, *Edisi ke Enam,* (Penterjemah K. Padmawinata). Bandung: Penerbit ITB.

Romruen, O., Karbowiak, T., Tongdeesoontorn, W., Shiekh, K.A., & Rawdkuen, S., 2022. Extraction and Characterization of Cellulose from Agricultural By-Products. *Polymers,* **14**(9): 1-13.

Rozikin, S., Amir, H., & Rohiat, S. 2018. Preparasi dan Karakterisasi Mikrokristalin Selulosa (MCC) Berbahan Baku Tandan Kosong Kelapa Sawit (Tkks). *Jurnal Pendidikan dan Ilmu Kimia*, **2**(1): 52-57.

Saba, N., Safwan, A., Sanyang, M. L., Mohammad, F., Pervaiz, M., Jawaid, M., Alothman, O. Y. & Sain, M., 2017. Thermal and Dynamic Mechanical Properties of Cellulose Nanofibers Reinforced Epoxy Composites. *International Journal of Biological Macromolecules.* **102**: 822-828.

Schwantes, D., Gonçalves Jr., A.C., Coelho, G.F., Campagnolo, M.A., Dragunski, D.C., Tarley, C.R.T., Miola, A.Jr., & Leismann, E.A.V., 2016, Chemical Modifications of Cassava Peel as Adsorbent Material for Metals Ions from Wastewater, *Hindawi J. Chem,* **16**: 1-15.

Sherlala, A. I. A., Raman, A. A. A., Bello, M. M., & Asghar, A., 2018. A review of the applications of organo-functionalized magnetic graphene oxide nanocomposites for heavy metal adsorption. *Chemosphere,* **193**: 1004-1017.

Sjostrom, E., 1995. *Kimia Kayu: Dasar-dasar dan Penggunaan*. *Jilid 2.* Yogyakarta: Universitas Gajah Mada Press.

Song, X., Wang, L., Ma, X., Zeng, Y., 2017. Adsorption Equilibrium and Thermodynamics of CO_2 and CH_4 on Carbon Molecular Sieves. *Applied Surface Science,* **396**: 870-878.

Susilowati, T., & Muljani, S., 2020. Synthesis of Cellulose Aerogel from Kapok Fiber for Cleaning The Waste of Lubricant Oil. *Jurnal Teknik Kimia,* **15**(1): 1-8.

Tanasale, Matheis F. J. D. P., Male, Yusthinus T., & Garium, N. B., 2020. Kinetika Adsorpsi Zat Warna Tartrazina Menggunakan Limbah Ampas Tahu sebagai Adsorben. *Fullerene Journal of chemistry*, **5**(2): 63-72.

Tang M., Jia R., Kan H., Liu Z., Yang S., Sun L., & Yang Y, 2020. Kinetic, Isotherm, and Thermodynamic Studies of The Adsorption of Dye From Aqueous

Solution by Propylene Glycol Adipate-Modified Cellulose Aerogel. *Colloids and Surfaces A: Physicochemical and Engineering Aspects*, **602**:125009.

Thaib, C. M., Erdiana, G., & Barita, A., 2020. Pembuatan Kertas dari Limbah Kulit Durian dan Ampas Tebu dengan Perbedaan Konsentrasi NaOH. *Jurnal Kimia Saintek dan Pendidikan*, **4**(1): 1-11.

Thakur, V., & Thakur, M.K., 2014. Processing and Characterization of Natural Cellulose Fibers/Thermoset Polymer Composites. *Carbohydrate Polymers*, **109**: 102-117.

Trilokesh, C. Uppuluri, & Kiran B., 2019. Isolation and Characterization of Cellulose Nanocrystals from Jack Fruit Peel, *Scientific Reports.* **9**(1): 1-8.

Vogel, Svehla, G., 1985. *Buku teks Analisis Anorganik Kualitatif Makro dan Semimikro, Edisi ke lima*. Jakarta.

Wan, C., Lu, Y., Jiao, Y., Sun, Q., & Li, J. 2015. Preparation, Characterization and Oil Adsorption Properties of Cellulose Aerogels from Four Kinds of Plant Materials via a NAOH/PEG Aqueous Solution. *Journal of Sol-Gel Science and Technology*, **74**(1): 256-259.

Wang, D., Zhang, G., Zhou, L., Wang, M., Cai, D., & Wu Z. 2017. Synthesis of a Multifunctional Graphene Oxide-Based Magnetic Nanocomposite for Efficient Removal of Cr(VI). Langmuir, **33**: 7007-7014.

Wang, J. & X. Guo, 2020. Adsorption Isotherm Models: Classification, Physical Meaning, Application and Solving Method. *Chemosphere*, **258**(127279): 1-79.

Wardani, A. R. K., 2016. Pengaruh Suhu dan Waktu Hidrotermal pada Sintesis Zeolit X berpendukung Serat Glasswool untuk Adsorpsi-Desopsi CO_2. Tesis Program Magister Kim-FMIPA-ITS.

Wei, W., Hu, H., Ji, X., Yan, Z., Sun, W., & Xie, J., 2018. Selective Adsorption of Organic Dyes by Porous Hydrophilic Silica Aerogels from Aqueous System. *Water Science and Technology*, **78**(2): 402-414.

Widiastuti, T, Afrizal, & Zulmanelis, 2016. Sintesis dan Karakterisasi Kertas Berbahan Dasar Selulosa Kulit Durian *(Durio Zibethinus)*. *Jurnal Risenologi Kpm UNJ*, **1**(2): 57-64.

Wu, H., Teng, C., Liu, B., Tian, H., Wang, J. G. 2018. Characterization and Long Term Antimicrobial Activity of The Nisin Anchored Cellulose Films. *International Journal of Biological Macromolecules*, **113**(1): 487-493.

Xiong, Y., Wang, C., Wang, H., Yao, Q., Fan, B., Chen, Y., Sun, Q., Jin, C., & Xu, X., 2017. 3D Titanate Aerogel with Cellulose as Adsorption-Aggregator for High Efficient Water Quality Purification. *J. Mater. Chem. A*, **5**(12): 5813-5819.

Xu, C., Zhu, S., Xing, C., Li, D., Zhu, N.,& Zhou, H., 2015. Isolation and Properties of Cellulose Nanofibrils from Coconut Palm Petioles by Different Mechanical Process. *PLoS One*, **10**(4): 0122123.

Xu, M., Bao, W., Xu, S., Wang, X., & Sun, R., 2016. Porous cellulose aerogels with high mechanical performance and their absorption behaviors. *BioResources*, **11**(1): 8-20.

Zaman, A., Huang, F., Jiang, M., Wei, W., & Zhou, Z., 2020. Preparation, Properties, and Applications of Natural Cellulosic Aerogels: A Review. *Energy and Built Environment,* **1**(1): 60-76.

Zhang, L., Luo, H., Liu, P., Fang, W., & Geng, J. 2016. A Novel Modified Graphene Oxide/chitosan Composite used as an Adsorbent for Cr(VI) in Aqueous Solutions. *Int J Biol Macromol,* **87**: 586-596.

Zhao, G., Lyu, X., Lee, J., Cui, X., & Chen, W.N., 2019. *Biodegradable and transparent cellulose film prepared eco-friendly from durian rind for packaging application. Food Packaging and Shelf Life.* **21**(100345):1-6.

Zhao, T., Chen, Z., Lin, X., Ren, Z., Li, B., & Zhang, Y. 2018. Preparation and characterization ofmi-crocrystalline cellulose (MCC) from tea waste, Carbohydr. Polym, **184**: 164–170.

Zhu, Z., Fu, S., & Lucia, L. A. 2019. A Fiber- Aligned Thermal-Managed Wood-Based Superhydrophobic Aerogel for Efficient Oil Recovery. *ACS Sustainable Chemistry & Engineering*, 7(19): 16428-16439.

Zhuang, J., Li, M., Pu, Y., Ragauskas, A. J.,& Chang, Y. G. 2020. Observation of Potential Contaminants in Processed Biomass Using Fourier Transform Infrared Spectroscopy. **10**(12): 1-13.

Zu, G., Shen, J., Zou, L., Wang, F., & Zhang, Y., 2016. Nanocellulose-Derived Highly Porous Carbon Aerogels for Supercapacitors. *Carbon*, **99:** 203-211**.**

Zulharmita, S. N. D., & Mahyuddin., 2012. Pembuatan Mikrokristalin Selulosa dari Ampas Tebu *(Saccharum Officinarum L.). Jurnal Sains dan Teknologi Farmasi*, **17**(2): 158-163.

Lampiran 1. Skema Preparasi sampel, *Dewaxing*, Delignifikasi, dan *Bleaching*

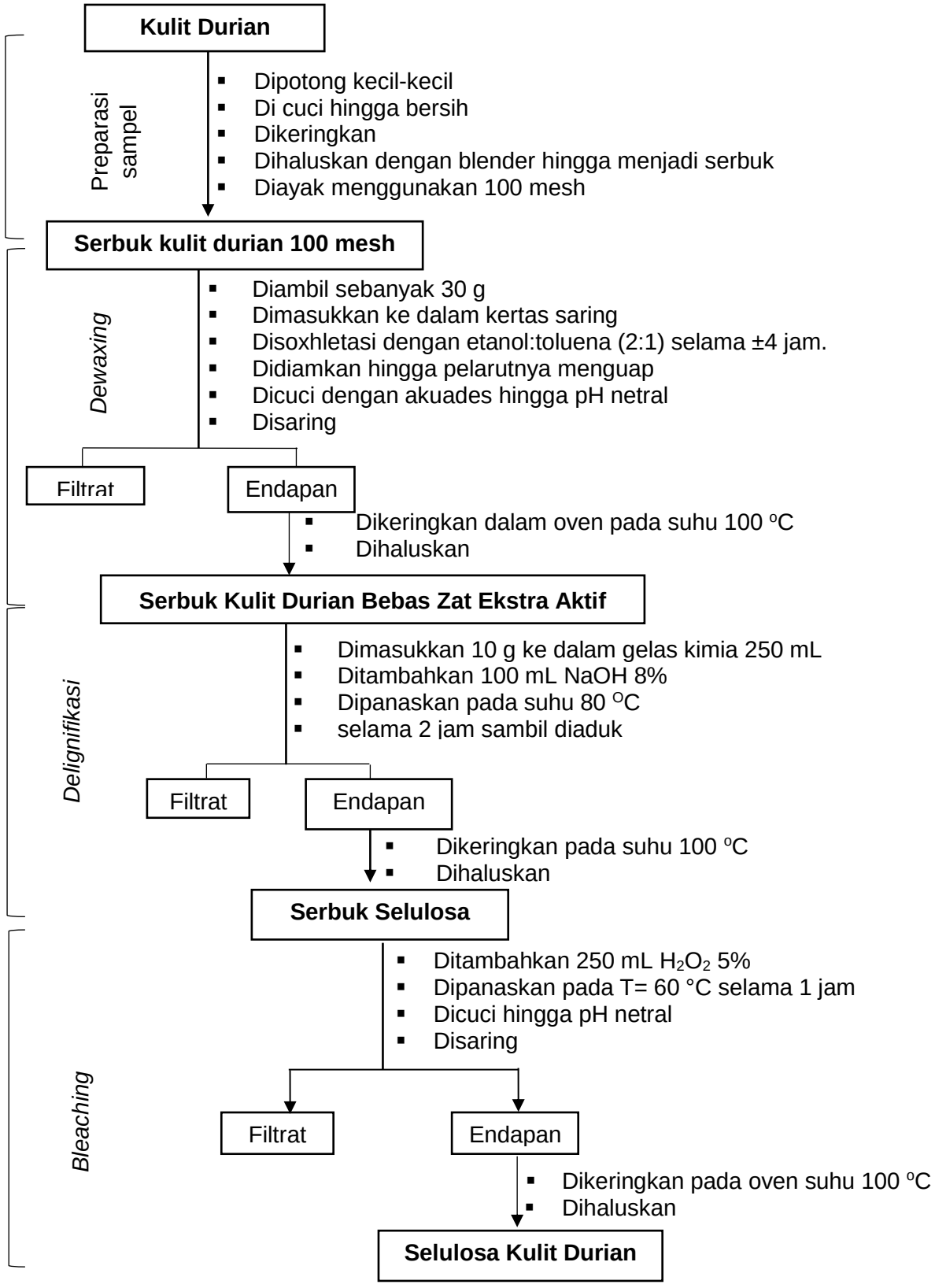

Lampiran 2. Skema Pembuatan Aerogel Selulosa

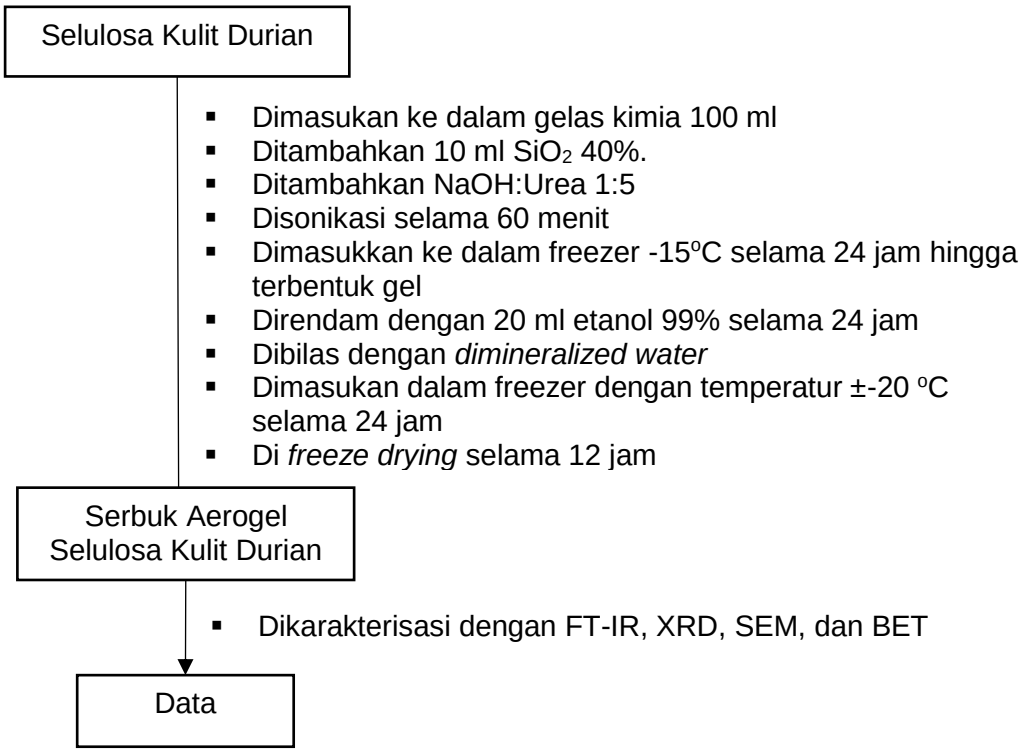

Lampiran 3. Penentuan Waktu Optimum pada Adsorpsi Ion Logam Cr(VI)

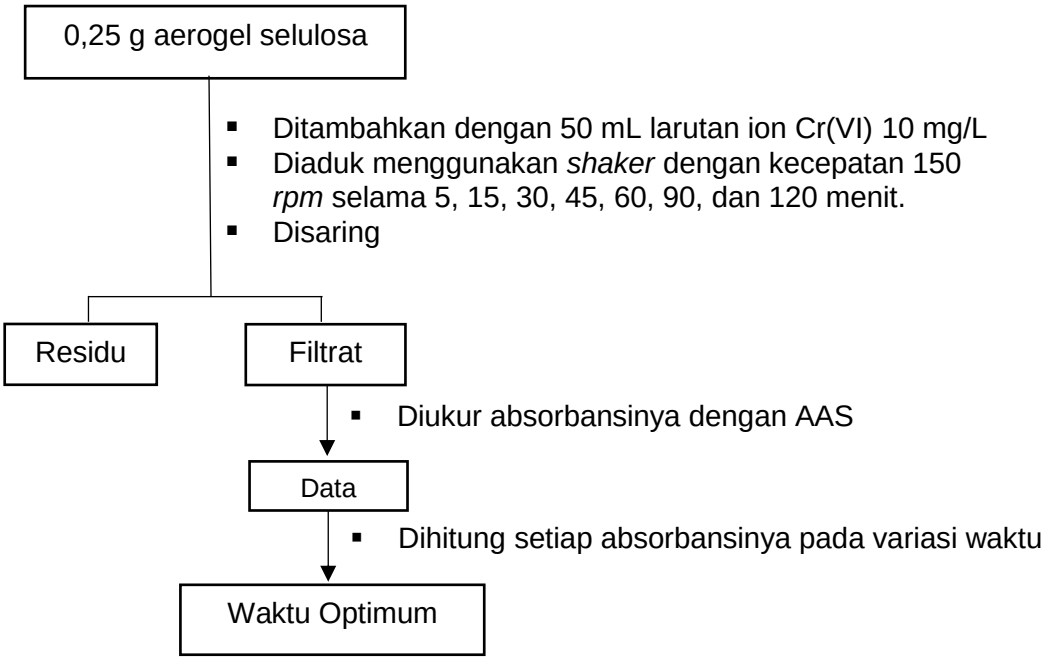

Lampiran 4. Penentuan pH Optimum pada Adsorpsi Ion Logam Cr(VI)

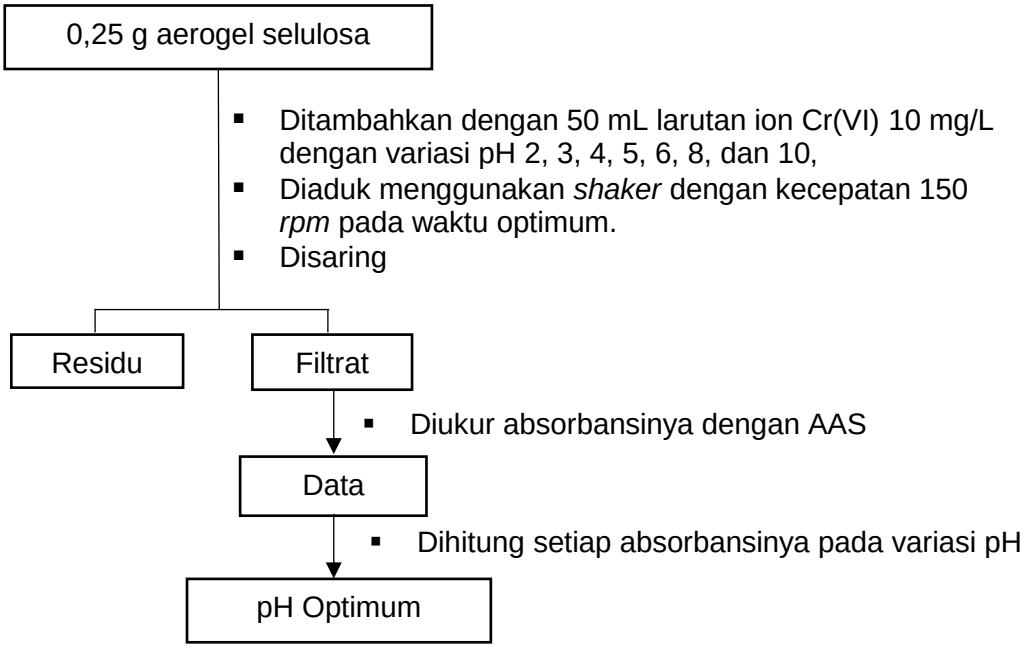

Lampiran 5. Penentuan Suhu Optimum pada Adsorpsi Ion Logam Cr(VI)

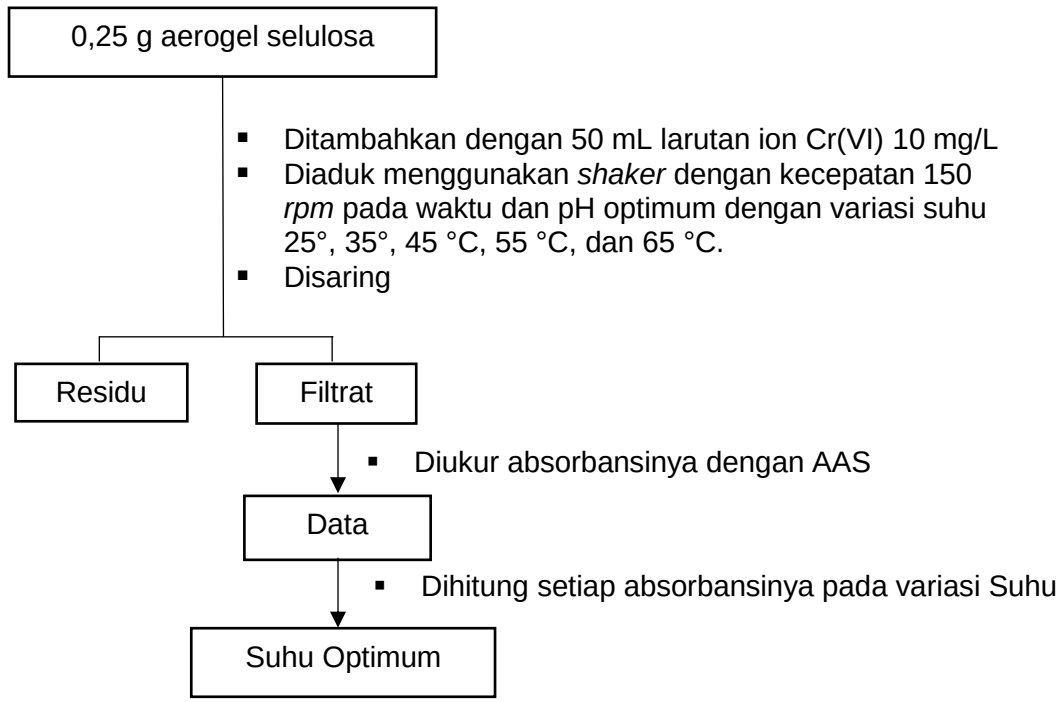

Lampiran 6. Penentuan Konsentrasi Optimum pada Proses Adsorpsi Ion Logam Cr(VI)

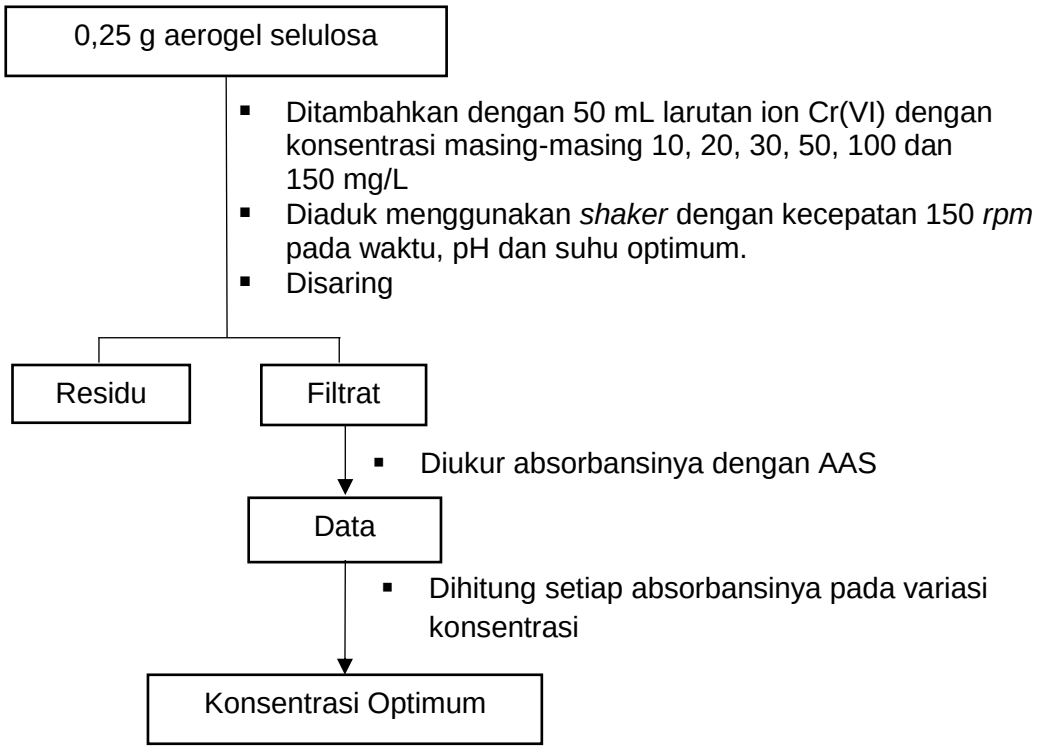

Lampiran 7. Dokumentasi Penelitian

1. Proses Ekstraksi Selulosa dari Kulit Durian

a) Preparasi sampel

Kulit Durian

Proses pengeringan Sampel

Serbuk Kulit Durian setelah diblender

b) Dewaxing

Preparasi sampel untuk di soxhlet

Proses Soxhlet

Sampel kulit durian setelah di soxhlet

c) Delignifikasi

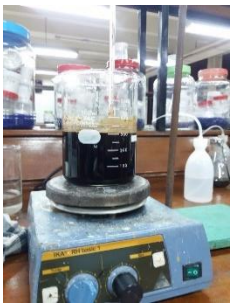

Proses delignifikasi menggunakan NaOH 8%

Proses Pencucian dan Penyaringan

Setelah dikeringkan dalam oven

d) Bleaching

Proses *bleaching* menggunakan H_2O_2 5%

Proses Pencucian dan Penyaringan Selulosa

Selulosa Kulit Durian

2. Proses Sintesis Aerogel Selulosa

Campuran selulosa+NaOH+Urea+SiO_2

Proses Sonikasi selama 60 menit

Setelah proses sonikasi

Campuran *difreezer* pada suhu -15 ^{0}C selama 1x24 jam

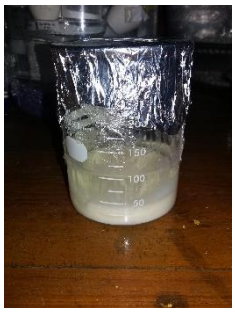

Perendaman dengan etanol 99% selama 24 jam

Aerogel setelah dibilas dengan *dimineralized water*

Setelah di*freezer* suhu ±-20 ^{o}C selama 24 jam

Aerogel selulosa di *freeze drying*

Aerogel Selulosa

3. Studi Adsorpsi

Larutan Cr(VI) 50 ppm

Proses penyaringan

Filtrat hasil penyaringan

Proses pengenceran

Larutan yang akan diukur absorbansinya menggunakan Spektrofotometer AAS

Lampiran 8. Perhitungan Rendemen (%) Selulosa Kulit Durian

Rendemen selulosa kulit durian dapat dihitung menggunakan persamaan berikut:

Rendemen (%) = $\frac{Bobot\ ekstrak\ yang\ diperoleh\ (g)}{Bobot\ Sampel\ Awal}$ x 100%

Maka, persentase rendemen selulosa pada proses ektraksi dari kulit durian yaitu:

- *Dewaxing*

Rendemen (%) = $\frac{22{,}755\ \text{g}}{30{,}117\ \text{g}}$ x 100%

= 77,55 %

- Delignifikasi

Rendemen (%) = $\frac{14{,}023\ \text{g}}{22{,}755\ \text{g}}$ x 100%

= 61,63 %

- *Bleaching*

Rendemen (%) = $\frac{12{,}250\ \text{g}}{14{,}023\ \text{g}}$ x 100%

= 87,36 %

Lampiran 9. Kurva Kalibrasi Ion Logam Cr(VI)

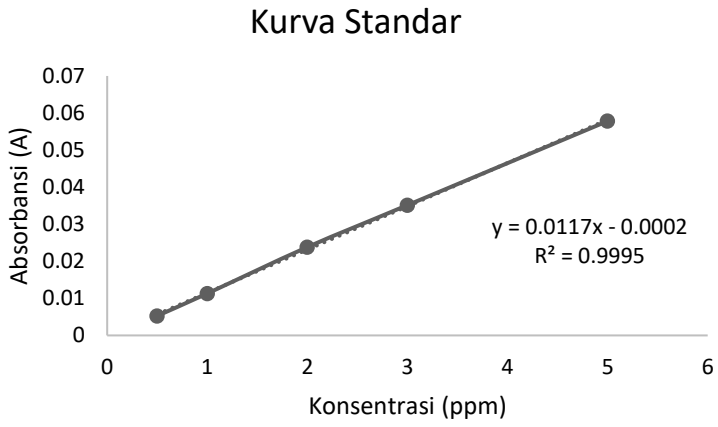

Gambar 28. Kurva Kalibrasi Logam Cr(VI)

Lampiran 10. Data Pengaruh Waktu terhadap adsorpsi Ion Logam Cr(VI)

Berdasarkan persamaan garis linear pada kurva kalibrasi Cr(VI), maka nilai C_e dapat dihitung menggunakan persamaan y = 0,0117x – 0,0002.

Contohnya:
Untuk waktu kontak 5 menit dengan absorbansi 0,02145 dan faktor pengenceran (FP) 5 kali.
Diketahui:

t = 5 menit
y = 0,02145
C_0 = 10,043 $mg.L^{-1}$
m = 0,2501 g
V = 0,05 L

Berdasarkan persamaan garis linear pada kurva standar, diperoleh:

y = 0,0117x - 0,0002
0,0215 = 0,0117x - 0,0002
0,0117x = 0,0215 + 0,0002
x = 1,850 $mg.L^{-1}$

Sehingga,

C_e = (nilai x) x Faktor Pengenceran
= 1,850 x 5
= 9,252 $mg.L^{-1}$

Selanjutnya, jumlah ion logam Cr(VI) yang teradsorpsi untuk t = 5 menit dapat dihitung menggunakan persamaan:

$$q_t = \frac{(C_0 - C_e)}{m} \text{ x V}$$

$$= \frac{(10{,}043 - 9{,}252)\ \text{mg.L}^{-1}}{0{,}2501\ \text{g}} \text{ x } 0{,}05 \text{ L}$$

= 0,1581 $mg.g^{-1}$

Jadi, jumlah ion logam Cr(VI) yang teradsorpsi oleh aerogel selulosa pada waktu kontak 5 menit adalah sebesar 0,1518 $mg.g^{-1}$

Dengan menggunakan perhitungan yang sama, maka jumlah ion logam Cr(VI) yang teradsorpsi untuk setiap variasi waktu kontak dapat ketahui. Berikut data hasil perhitungan untuk penentuan waktu kontak optimum ion logam Cr(VI) dapat dilihat pada Tabel 10.

Tabel 10. Data penentuan waktu optimum ion logam Cr(VI) oleh Aerogel Selulosa

t (m)	m (g)	C_o (mg.L^{-1})	C_e (mg.L^{-1})	V (L)	q_t (mg.g^{-1})
5	0,2501	10,043	9,252	0,05	0,158
15	0,2501	10,043	8,846	0,05	0,239
30	0,2501	10,043	8,675	0,05	0,273
45	0,2501	10,043	8,479	0,05	0,313
60	0,2502	10,043	8,543	0,05	0,300
90	0,2501	10,043	8,530	0,05	0,302
120	0,2502	10,043	8,551	0,05	0,298

Lampiran 11. Data Pengaruh pH terhadap adsorpsi Ion Logam Cr(VI) (t = 45 menit)

Rumus Perhitungan jumlah ion logam Cr(VI) yang teradsorpsi:

$$q_t = \frac{(C_0 - C_e)}{m} \text{ x } V$$

Tabel 11. Data penentuan pH optimum Ion Logam Cr(VI) oleh Aerogel Selulosa

pH	m (g)	C_o (mg.L^{-1})	C_e (mg.L^{-1})	V (L)	q_t (mg.g^{-1})
2	0,2501	9,915	7,607	0,05	0,4614
3	0,2501	10,043	8,333	0,05	0,3417
4	0,2501	7,350	5,940	0,05	0,2819
5	0,2501	9,231	8,547	0,05	0,1367
6	0,2501	6,752	6,453	0,05	0,0598
8	0,2501	5,940	5,769	0,05	0,0342
10	0,2501	6,175	6,047	0,05	0,0256

Lampiran 12. Data Pengaruh suhu terhadap adsorpsi Ion Logam Cr(VI) (t = 45 menit, pH = 2)

Rumus Perhitungan jumlah ion logam Cr(VI) yang teradsorpsi:

$$q_t = \frac{(C_0 - C_e)}{m} \text{ x } V$$

Tabel 12. Data penentuan Suhu optimum Ion Logam Cr(VI) oleh Aerogel Selulosa

Suhu (°C)	m (g)	C_o (mg.L^{-1})	C_e (mg.L^{-1})	V (L)	q_t (mg.g^{-1})
25	0,2501	10,171	8,974	0,05	0,239
35	0,2501	9,915	8,162	0,05	0,350
45	0,2501	10,556	8,162	0,05	0,478
55	0,2501	10,769	8,462	0,05	0,461
65	0,2501	10,513	8,590	0,05	0,384

Lampiran 13. Data Pengaruh Konsentrasi terhadap adsorpsi Ion Logam Cr(VI) (t = 45 menit, pH = 2, T = 45 °C)

Rumus Perhitungan jumlah ion logam Cr(VI) yang teradsorpsi:

$$q_t = \frac{(C_0 - C_e)}{m} \text{ x } V$$

Tabel 13. Data penentuan Konsentrasi optimum Ion Cr(VI) oleh Aerogel Selulosa

Konsentrasi (mg.L^{-1})	m (g)	C_o (mg.L^{-1})	C_e (mg.L^{-1})	V (L)	q_t (mg.g^{-1})
10	0,2501	9,957	7,564	0,05	0,478
20	0,2501	19,231	14,701	0,05	0,906
30	0,2501	23,248	17,863	0,05	1,077
50	0,2501	50,427	39,744	0,05	2,137
100	0,2501	89,103	72,650	0,05	3,291
150	0,2501	148,718	125,427	0,05	4,658

Lampiran 14. Studi Model Kinetika Adsorpsi Ion Logam Cr(VI)

Kinetika orde satu semu dapat dihitung menggunakan persamaan berikut:

$\ln (q_e - q_t) = -k_1 t + \ln q_e$

Tabel 14. Data Studi Kinetika Adsorpsi Ion Logam Cr(VI) oleh Aerogel Selulosa

t (m)	q_e (mg.g^{-1})	q_t (mg.g^{-1})	$q_e - q_t$	$\ln (q_e - q_t)$	t/q_t
5	0,3127	0,1581	0,155	-1,867	31,634
15	0,3127	0,2392	0,073	-2,611	62,703
30	0,3127	0,2734	0,039	-3,237	109,731
45	0,3127	0,3127	0,000	0,000	143,910
60	0,3127	0,2998	0,013	-4,348	200,159
90	0,3127	0,3024	0,010	-4,580	297,576
120	0,3127	0,2981	0,015	-4,224	402,613

Jika di Plot $\ln (q_e - q_t)$ terhadap t, maka *slope* adalah -k dan Intersep adalah ln qe, sehingga diperoleh persamaan garis lurus:

y = -0,0232x - 1,7716

Dari persamaan garis diatas, maka diperoleh nilai slope (a) = -0,0232 dan nilai intersep (b) = 1,7716, sehingga nilai k_1 dapat dihitung sebagai berikut:

Slope = - *k*

k_1 = - slope

= - (-0,0232)

= 0,0232 menit^{-1}

Nilai adsorpsi dapat dihitung sebagai berikut :

Intersep = ln q_e

q_e = $e^{intersep}$

= $e^{3,0888}$

= 0,1701 mg.g^{-1}

k_1 = 0,0232 menit^{-1}

R^2 = 0,3379

Rumus kinetika orde dua semu dapat dihitung menggunakan persamaan berikut:

$$\frac{t}{q_t} = \frac{1}{k_2 q_e^2} + \frac{1}{q_e} t$$

Jika di Plot t/qt terhadap t (waktu), maka slope adalah 1/qe dan Intersep adalah $1/k_2qe^2$, sehingga diperoleh persamaan garis lurus:

Dari grafik kinetika orde dua semu diperoleh persamaan garis

y = 3,2101x + 10,05

dari persamaan garis diperleh nilai slope (a) = 3,2101 dan intercept (b) = 10,05 nilai k_2 diperoleh sebagai berikut:

slope = $\frac{1}{q_e}$

q_e = $\frac{1}{slope}$

= $\frac{1}{3,2101}$

= 0,3115 mg.g^{-1}

Intercept = $\frac{1}{k_2 {q_e}^2}$

k_2 $= \frac{1}{q_e{}^2.\text{intercept}}$

$= \frac{1}{(0{,}3115)^2 \text{ x } 10{,}05}$

$= 0{,}2932 \text{ g.mg}^{-1}\text{menit}^{-1}$

k_2 $= 0{,}2932 \text{ g.mg}^{-1}\text{menit}^{-1}$

R^2 $= 0{,}9978$

Lampiran 15. Penentuan Kapasitas dan Isothermal Adsoprsi Ion Logam Cr(VI)

- Persamaan adsorpsi Isotermal Langmuir:

$$\frac{C_e}{q_e} = \frac{1}{Q_o b} + \frac{C_e}{Q_o}$$

Tabel 15. Data Isothermal Langmuir terhadap adsorpsi ion logam Cr(VI) oleh aerogel selulosa

Co ($mg.L^{-1}$)	Ce ($mg.L^{-1}$)	q_e ($mg.g^{-1}$)	Ce/qe
10	9,957	0,478	15,810
20	19,231	0,906	16,226
30	23,248	1,077	16,587
50	50,427	2,137	18,600
100	89,103	3,291	22,078
150	148,718	4,658	26,927

Jika di plot Ce/qe terhadap Ce, maka slope adalah $1/Q_o$ dan Intersep adalah $1/Q_o b$, sehingga diperoleh persamaan garis lurus:

Berdasarkan model Isotermal Langmuir diperoleh persamaan garis

y = 0,0961x + 14,918

dari persamaan garis diperoleh nilai slope (a) = 0,0961 dan intercept (b) = 14,918

$\frac{1}{Q_o}$ = slope

Q_o $= \frac{1}{\text{slope}}$

$= \frac{1}{0{,}0961}$

$= 10{,}4058 \text{ mg.g}^{-1}$

Intensitas adsorpsi dapat dihitung sebagai berikut :

$\frac{1}{Q_o.b}$ = intercept

b = $\frac{1}{Q_o.\text{intercept}}$

= $\frac{1}{10{,}4058 \text{ x } 14{,}918}$

= 0,0064 L.mg^{-1}

Tabel 16. Data Isotermal Freundlich terhadap adsorpsi ion logam Cr(VI) oleh aerogel selulosa

Co (mg.L^{-1})	Ce (mg.L^{-1})	q_e (mg.g^{-1})	Log Ce	Log qe
10	9,957	0,478	0,879	-0,320
20	19,231	0,906	1,167	-0,043
30	23,248	1,077	1,252	0,032
50	50,427	2,137	1,599	0,330
100	89,103	3,291	1,861	0,517
150	148,718	4,658	2,098	0,668

Contoh perhitungan nilai parameter isotermal Freundlich sebagai berikut:

Persamaan adsorpsi isothermal Freundlich yaitu:

$$\text{Log } q_e = \text{Log } k + \frac{1}{n} \text{Log } C_e$$

Jika di Plot log qe terhadap Log Ce, maka slope adalah 1/n dan Intersep adalah Log k, sehingga diperoleh persamaan garis lurus:

$$y = 0{,}8098x - 0{,}9981$$

dari persamaan garis tersebut diperoleh nilai slope (a) = 0,8098 dan nilai intersep (b) = 0,9981

Nilai kapasitas adsorpsi dapat dihitung sebagai berikut:

log k_f = intercept

k_f = invers log intercept

= invers log 0,9981

k_f = 9,956 mg/g

Intensitas adsorpsi dapat dihitung sebagai berikut

$\frac{1}{n}$ = slope

n = $\frac{1}{\text{slope}}$

$= \frac{1}{0{,}8098\ \mathrm{L/g}}$

= 1,2349 g/L

Lampiran 16. Penentuan Termodinamika Adsoprsi Ion Logam Cr(VI)

Parameter termodinamika adsorpsi terdiri dari perubahan entalpi ($\Delta H°$), perubahan entropi ($\Delta S°$), dan perubahan energi bebas Gibbs ($\Delta G°$) yang masing-masing dapat dihitung menggunakan persamaan di bawah ini:

$$\ln \mathrm{Kc} = -\frac{\Delta S^o}{\mathrm{R}} \cdot \frac{\Delta H^o}{\mathrm{RT}}$$

$$\mathrm{K_c} = \frac{\mathrm{qe}}{\mathrm{Ce}}$$

$$\Delta G^0 = \Delta H^0 - T\Delta S^0$$

Tabel 17. Data Parameter Termodinamika (ΔG^0, ΔH^0, dan ΔS^0)

T (K)	1/T	qe/ce	In K_c	ΔG^o	ΔH^o	ΔS^o
298	0,00336	0,0267	-3,62474	-2699,74		
308	0,00325	0,0508	-2,98005	-2790,71		
318	0,00314	0,0699	-2,66044	-2881,68	+11,133	+9,097
328	0,00305	0,0584	-2,83979	-2972,65		
338	0,00296	0,0485	-3,0269	-3063,62		

Dari grafik plot antara 1/T terhadap In Kc, diperoleh persamaan garis y = -1339x + 1,0941. Maka slope (a) = -1339 dan nilai intersep (b) = 1,0941

Sehingga, nilai ΔH dapat dihitung:

$\frac{\Delta H^o}{\mathrm{R}}$ = slope

$\frac{\Delta H^o}{8{,}3145}$ = -(-1339)

ΔH^o = 11,133

Nilai ΔS diperoleh dari:

$\frac{\Delta S^o}{\mathrm{R}}$ = intercept

$\frac{\Delta S^o}{8{,}3145}$ = 1,0941

ΔS^o = 9,097

Penentuan jumlah energi Gibbs (ΔG^0) menggunakan persamaan:

$$\Delta G^0 = \Delta H^0 - T\Delta S^0$$

Untuk T = 298 K

$\Delta G^0 = \Delta H^0 - T\Delta S^0$

= 11,133 – (298 K x 9,097)

= -2699,77 J

= -2,6997 kJ

Untuk T = 328 K

$\Delta G^0 = \Delta H^0 - T\Delta S^0$

= 11,133 – (328 K x 9,097)

= -2972,6 J

= -2,9726 kJ

Untuk T = 308 K

$\Delta G^0 = \Delta H^0 - T\Delta S^0$

= 11,133 – (308 K x 9,097)

= -2790,7 J

= -2,7907 kJ

Untuk T = 338 K

$\Delta G^0 = \Delta H^0 - T\Delta S^0$

= 11,133 – (338 K x 9,097)

= -3063,6 J

= -3,0636 kJ

Untuk T = 318 K

$\Delta G^0 = \Delta H^0 - T\Delta S^0$

= 11,133 – (318 K x 9,097)

= -2,8816 J

= -2,8816 kJ

Lampiran 17. Hasil Analisis FTIR

SHIMADZU

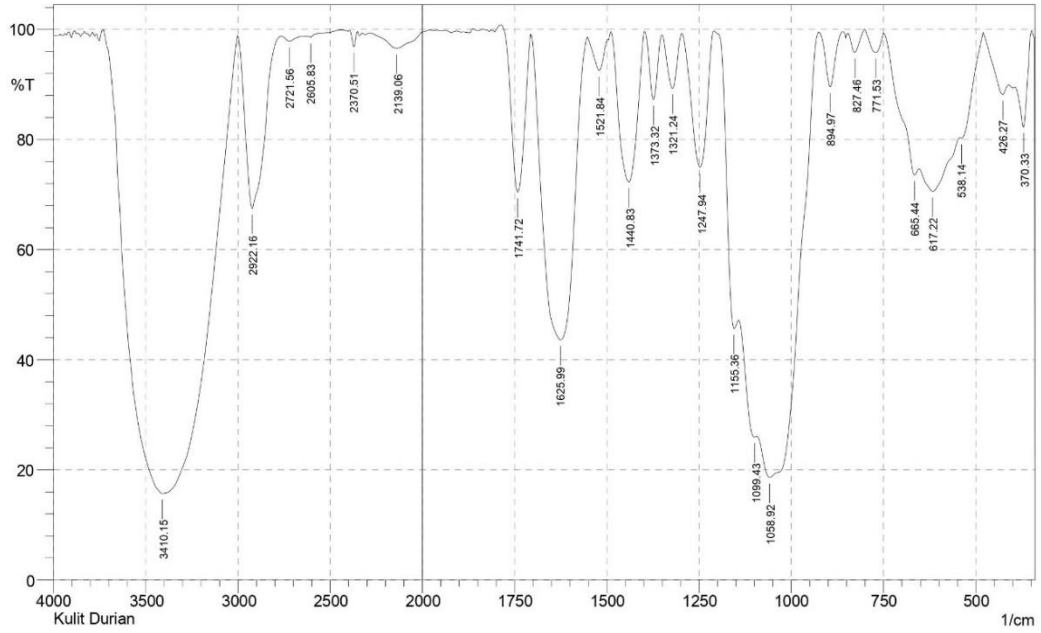

	Peak	Intensity	Corr. Intensity	Base (H)	Base (L)	Area	Corr. Area
1	370.33	82.281	12.599	393.48	349.12	2.324	1.283
2	426.27	88.167	3.833	478.35	410.84	2.411	0.677
3	538.14	80.266	1.237	542	480.28	3.203	0.309
4	617.22	70.573	5.86	651.94	543.93	14.097	2.108
5	665.44	73.564	4.103	748.38	653.87	7.098	0.853
6	771.53	95.801	3.841	800.46	750.31	0.586	0.519
7	827.46	95.832	3.766	846.75	800.46	0.457	0.388
8	894.97	89.568	9.942	923.9	862.18	1.351	1.221
9	1058.92	18.655	22.64	1093.64	925.83	75.6	27.321
10	1099.43	25.972	1.868	1141.86	1095.57	22.241	1.089
11	1155.36	45.696	10.761	1209.37	1143.79	10.425	1.376
12	1247.94	75.002	24.498	1296.16	1211.3	5.604	5.411
13	1321.24	89.296	9.802	1350.17	1298.09	1.458	1.251
14	1373.32	87.246	12.024	1398.39	1352.1	1.396	1.251
15	1440.83	72.288	27.109	1487.12	1400.32	7.358	7.13
16	1521.84	92.565	5.682	1550.77	1498.69	1.116	0.719
17	1625.99	43.624	55.209	1705.07	1552.7	30.939	30.166
18	1741.72	70.448	29.392	1786.08	1707	5.689	5.663
19	2139.06	96.578	3.001	2279.86	1980.89	2.595	2.069
20	2370.51	96.904	2.784	2395.59	2353.16	0.296	0.242
21	2605.83	98.553	0.348	2625.12	2524.82	0.397	0
22	2721.56	97.828	0.923	2763.99	2654.05	0.806	0.204
23	2922.16	67.52	31.231	3001.24	2765.92	18.775	17.491
24	3410.15	15.715	83.759	3730.33	3003.17	314.645	312.752

Comment;
Kulit Durian

Date/Time; 10/13/2021 3:36:24 PM
No. of Scans;
Resolution;
Apodization;

SHIMADZU

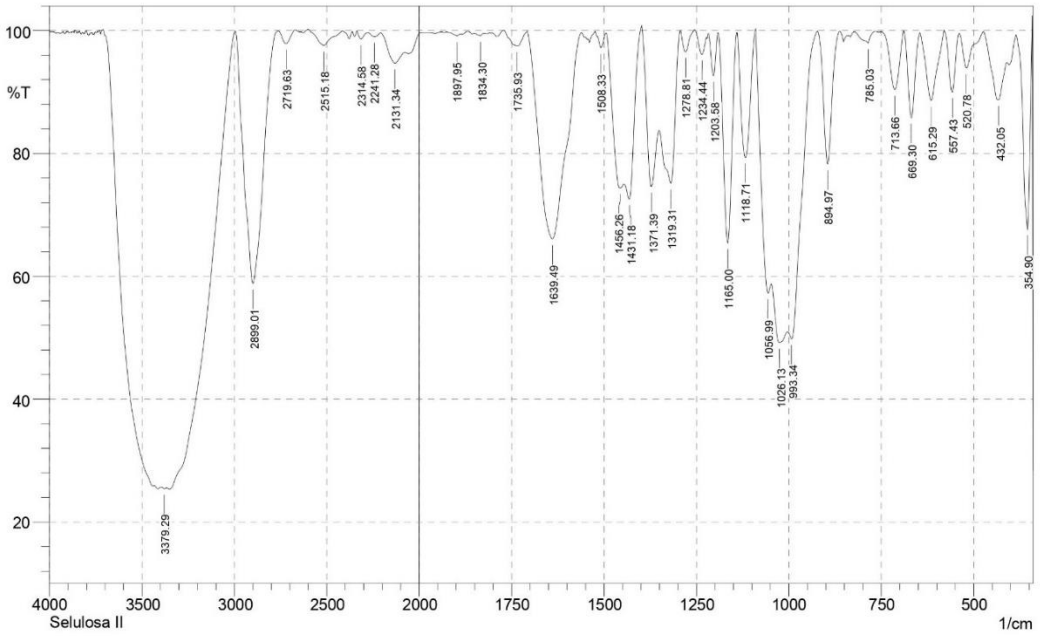

No.	Peak	Intensity	Corr. Intensity	Base (H)	Base (L)	Area	Corr. Area
1	354.9	67.686	30.074	383.83	343.33	3.254	2.913
2	432.05	88.727	7.796	472.56	410.84	1.961	1.198
3	520.78	93.931	5.683	540.07	474.49	0.805	0.711
4	557.43	90.009	9.742	580.57	540.07	0.884	0.846
5	615.29	88.625	11.051	644.22	580.57	1.726	1.648
6	669.3	85.82	13.963	688.59	646.15	1.366	1.322
7	713.66	90.389	9.483	750.31	690.52	1.243	1.207
8	785.03	97.941	1.9	823.6	767.67	0.257	0.217
9	894.97	78.256	21.618	921.97	864.11	2.54	2.508
10	993.34	49.813	7.079	1002.98	923.9	10.915	0.959
11	1026.13	49.219	5.635	1047.35	1004.91	12.228	1.056
12	1056.99	57.274	9.275	1089.78	1049.28	6.428	1.529
13	1118.71	79.329	20.428	1139.93	1091.71	2.705	2.659
14	1165	65.446	34.153	1190.08	1141.86	4.39	4.305
15	1203.58	92.641	6.934	1217.08	1192.01	0.459	0.412
16	1234.44	96.097	3.25	1255.66	1222.87	0.312	0.245
17	1278.81	96.521	3.539	1294.24	1255.66	0.269	0.282
18	1319.31	75.152	17.547	1350.17	1294.24	4.694	2.61
19	1371.39	74.589	16.24	1398.39	1352.1	3.793	2.008
20	1431.18	72.556	10.139	1444.68	1400.32	3.552	0.986
21	1456.26	74.399	5.515	1494.83	1446.61	4.036	0.898
22	1508.33	97.207	2.51	1523.76	1494.83	0.195	0.16
23	1639.49	66.063	33.691	1707	1562.34	13.455	13.293
24	1735.93	97.496	0.139	1772.58	1734.01	0.252	0.042
25	1834.3	99.145	0.384	1851.66	1826.59	0.07	0.019
26	1897.95	99.112	0.416	1926.89	1886.38	0.096	0.026
27	2131.34	94.675	3.075	2208.49	2079.26	2.04	0.922
28	2241.28	99.014	0.678	2279.86	2208.49	0.217	0.122
29	2314.58	98.63	1.208	2337.72	2279.86	0.205	0.158
30	2515.18	97.556	2.515	2600.04	2416.81	0.919	0.969
31	2719.63	97.876	2.123	2762.06	2669.48	0.428	0.431
32	2899.01	58.825	41.047	2993.52	2763.99	23.94	23.818
33	3379.29	25.416	0.206	3394.72	3367.71	16.015	0.048

Date/Time; 12/29/2021 2:24:54 PM
No. of Scans;

SHIMADZU

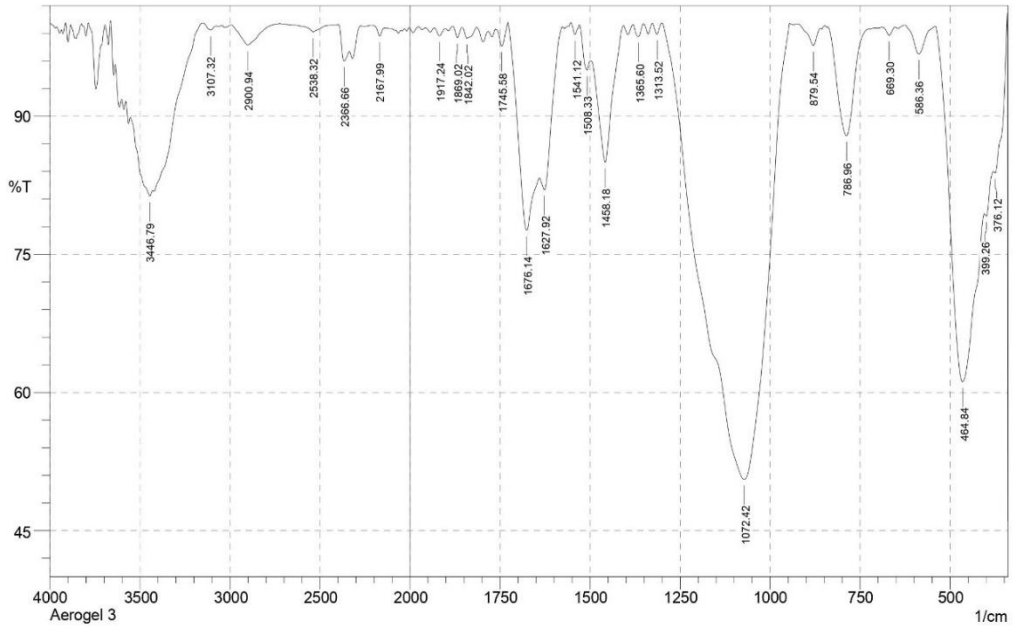

No.	Peak	Intensity	Corr. Intensity	Base (H)	Base (L)	Area	Corr. Area
1	376.12	83.82	0.979	378.05	343.33	1.815	0.5
2	399.26	79.162	0.97	403.12	379.98	2.029	0.042
3	464.84	61.163	27.266	540.07	405.05	17.403	10.482
4	586.36	96.766	3.078	624.94	540.07	0.538	0.478
5	669.3	98.774	0.901	688.59	651.94	0.115	0.064
6	786.96	87.899	11.688	839.03	725.23	2.902	2.693
7	879.54	97.667	2.017	923.9	860.25	0.292	0.232
8	1072.42	50.558	49.479	1300.02	947.05	53.336	53.422
9	1313.52	98.904	1.209	1327.03	1300.02	0.055	0.069
10	1365.6	98.644	1.36	1381.03	1352.1	0.096	0.096
11	1458.18	84.994	12.698	1498.69	1408.04	3.245	2.417
12	1508.33	95.003	2.214	1529.55	1498.69	0.459	0.179
13	1541.12	98.844	1.2	1552.7	1529.55	0.056	0.061
14	1627.92	82.017	4.323	1639.49	1577.77	2.904	0.555
15	1676.14	77.622	12.472	1726.29	1641.42	6.008	2.548
16	1745.58	97.618	2.191	1762.94	1728.22	0.192	0.163
17	1842.02	98.46	1.197	1855.52	1815.02	0.185	0.125
18	1869.02	98.52	1.188	1882.52	1855.52	0.095	0.061
19	1917.24	98.735	0.812	1932.67	1901.81	0.112	0.052
20	2167.99	98.694	0.99	2214.28	2140.99	0.191	0.103
21	2366.66	95.985	2.468	2397.52	2337.72	0.718	0.323
22	2538.32	99.133	0.837	2723.49	2418.74	0.35	0.333
23	2900.94	97.718	2.239	2993.52	2725.42	1.119	1.098
24	3107.32	99.331	0.594	3151.69	3074.53	0.107	0.09
25	3446.79	81.327	1.711	3552.88	3429.43	9.165	0.923

Comment;

Aerogel 3

Date/Time; 2/14/2022 3:46:53 PM

No. of Scans;

Resolution;

Apodization;

SHIMADZU

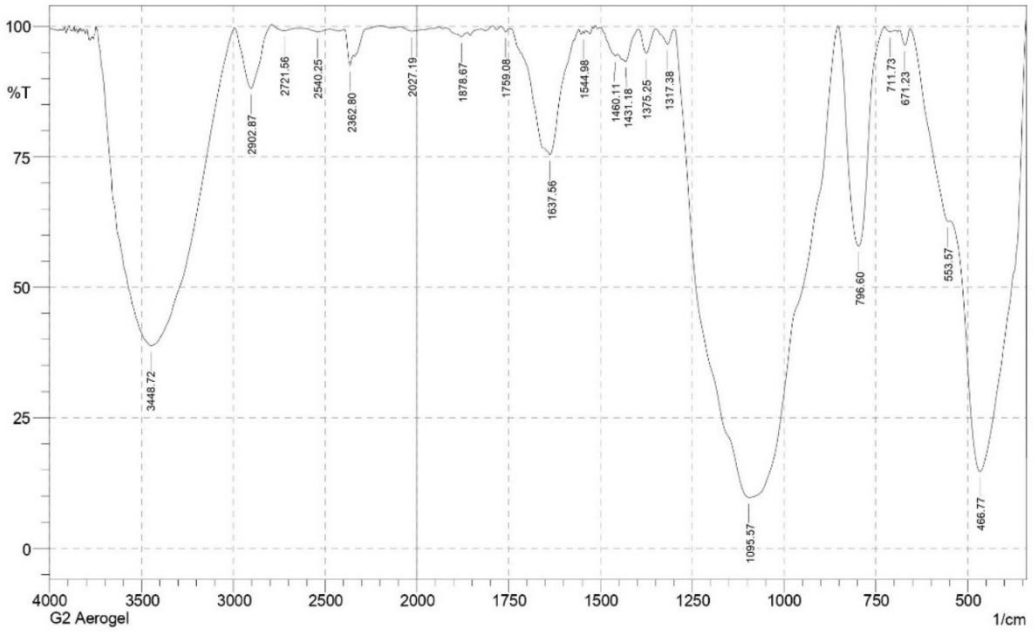

No.	Peak	Intensity	Corr. Intensity	Base (H)	Base (L)	Area	Corr. Area
1	466.77	14.692	62.048	545.85	343.33	90.515	69.581
2	553.57	62.612	2.055	655.8	547.78	11.635	0.637
3	671.23	96.4	2.999	686.66	655.8	0.282	0.201
4	711.73	98.96	0.603	727.16	696.3	0.105	0.047
5	796.6	57.883	42.139	852.54	727.16	13.397	13.404
6	1095.57	9.726	89.955	1298.09	854.47	212.931	212.371
7	1317.38	96.597	2.854	1350.17	1300.02	0.411	0.294
8	1375.25	94.816	4.666	1396.46	1350.17	0.58	0.476
9	1431.18	93.228	1.554	1438.9	1396.46	0.719	0.073
10	1460.11	94.316	1.021	1498.69	1454.33	0.679	0.131
11	1544.98	98.654	0.376	1546.91	1539.2	0.036	0.005
12	1637.56	75.428	2.387	1643.35	1573.91	4.53	0.293
13	1759.08	98.898	0.897	1772.58	1749.44	0.055	0.037
14	1878.67	97.958	1.044	1923.03	1863.24	0.325	0.124
15	2027.19	99.031	0.304	2090.84	2007.9	0.218	0.048
16	2362.8	92.47	3.778	2393.66	2345.44	1.063	0.389
17	2540.25	98.877	0.685	2621.26	2474.67	0.461	0.188
18	2721.56	99.121	0.863	2789.07	2665.62	0.271	0.282
19	2902.87	88.106	11.891	2993.52	2791	5.296	5.325
20	3448.72	38.759	60.744	3739.97	2995.45	169.128	167.639

Comment;
G2 Aerogel

Date/Time; 7/1/2022 10:18:13 AM
No. of Scans;
Resolution;
Apodization;

SHIMADZU

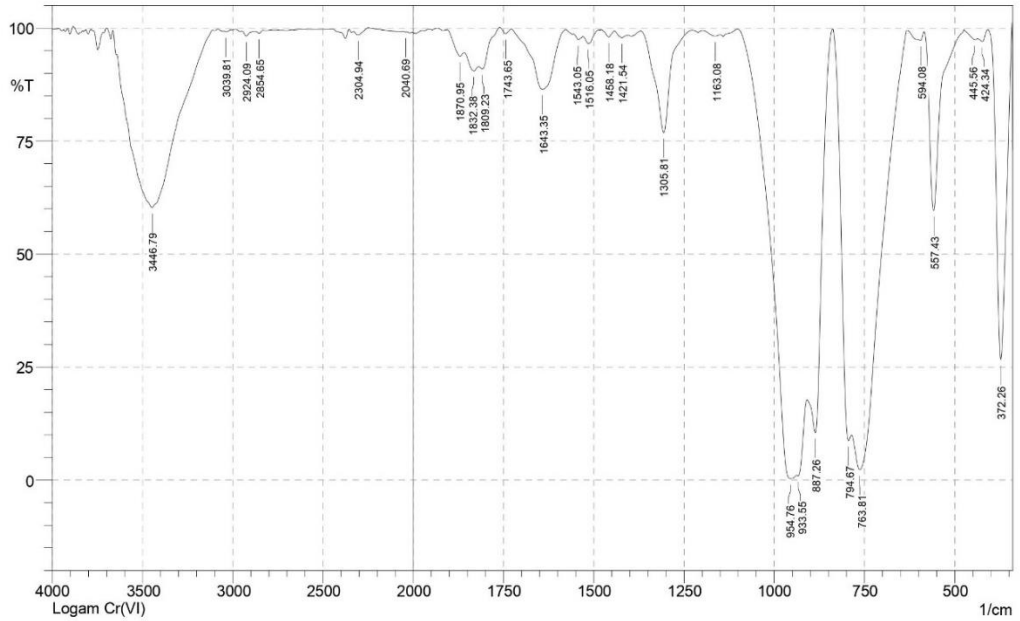

No.	Peak	Intensity	Corr. Intensity	Base (H)	Base (L)	Area	Corr. Area
1	372.26	26.661	71.883	406.98	343.33	14.221	13.83
2	424.34	97.034	1.538	437.84	408.91	0.272	0.1
3	445.56	97.452	0.616	474.49	437.84	0.272	0.055
4	557.43	59.663	39.671	584.43	474.49	7.108	6.843
5	594.08	97.296	1.983	632.65	584.43	0.387	0.252
6	763.81	2.264	20.303	785.03	634.58	86.685	22.132
7	794.67	8.729	15.002	837.11	786.96	24.322	2.459
8	887.26	10.472	32.35	908.47	839.03	31.723	8.662
9	933.55	0.942	2.491	937.4	910.4	35.53	1.716
10	954.76	0.316	10.114	1101.35	939.33	101.329	11.883
11	1163.08	98.245	0.53	1197.79	1149.57	0.274	0.06
12	1305.81	76.86	22.574	1369.46	1230.58	5.296	4.958
13	1421.54	97.853	0.993	1442.75	1406.11	0.259	0.086
14	1458.18	97.999	1.494	1479.4	1442.75	0.187	0.11
15	1516.05	96.58	2.038	1529.55	1487.12	0.401	0.192
16	1543.05	97.432	0.988	1556.55	1529.55	0.242	0.055
17	1643.35	86.492	13.234	1728.22	1579.7	4.316	4.147
18	1743.65	98.777	1.187	1761.01	1728.22	0.088	0.084
19	1809.23	90.98	1.972	1818.87	1762.94	1.139	0.167
20	1832.38	90.506	1.905	1857.45	1820.8	1.369	0.194
21	1870.95	93.755	2.087	1905.67	1859.38	0.822	0.226
22	2040.69	99.13	0.062	2056.12	2034.9	0.074	0.003
23	2304.94	98.477	1.082	2331.94	2250.93	0.315	0.208
24	2854.65	98.842	0.554	2873.94	2831.5	0.157	0.047
25	2924.09	98.264	1.059	2949.16	2873.94	0.355	0.129
26	3039.81	99.168	0.235	3049.46	3008.95	0.113	0.021
27	3446.79	60.279	35.824	3641.6	3113.11	60.324	52.836

Comment;
Logam Cr(VI)

Date/Time; 10/26/2022 3:44:13 PM
No. of Scans;
Resolution;
Apodization;

Lampiran 18. Hasil Analisis XRD

a. Kulit durian

Match! Phase Analysis Report

Sample: KULIT-DURIAN (2-80)

Sample Data

File name	KULIT-DURIAN.RAW
File path	D:/xrd/KULIT-DURIAN
Data collected	Feb 8, 2023 18:12:28
Data range	2.000° - 80.000°
Original data range	2.000° - 80.000°
Number of points	3901
Step size	0.020
Rietveld refinement converged	No
Alpha2 subtracted	No
Background subtr.	No
Data smoothed	Yes
Radiation	X-rays
Wavelength	1.540600 Å

Candidates

Name	*Formula*	*Entry No.*	*FoM*
Iron	Fe	96-901-3476	0.6773
Chromium	Cr	96-500-0221	0.6746
Chromium	Cr	96-900-8532	0.6746
(Fe0.95 W0.05)	Fe0.95 W0.05	96-152-2088	0.6734
(Fe0.75 V0.25)	Fe0.75 V0.25	96-152-3401	0.6688
Iron	Fe	96-901-3481	0.6688
(Au0.05 Fe0.95)	Au0.05 Fe0.95	96-151-0056	0.6682
	Fe0.915 Re0.085	96-152-3168	0.6678
Iron	Fe	96-901-3479	0.6676
Iron	Fe	96-901-3480	0.6676
(Fe0.97 Pd0.03)	Fe0.97 Pd0.03	96-152-3167	0.6657
Iron	Fe	96-901-3482	0.6643
Iron	Fe	96-901-3478	0.6617
(Fe0.9 Ru0.1)	Fe0.9 Ru0.1	96-152-3150	0.6611
Periclase	Mg O	96-901-3219	0.6544
	Fe	96-720-4905	0.6507
Iron	Fe	96-901-3477	0.6502
(Cu (N H3)4)3 (Sc F6)2	Cu3 F12 H36 N12 Sc2	96-152-5697	0.6499
(Fe0.94 Rh0.06)	Fe0.94 Rh0.06	96-152-3169	0.6491
	Mo2 O15 P4	96-430-3257	0.6458
Niobium oxo phosphate	Nb2 O15 P4	96-434-5204	0.6457
Periclase	Mg O	96-901-3252	0.6436
(Fe0.95 Ru0.05)	Fe0.95 Ru0.05	96-152-2769	0.6372
Periclase	Mg O	96-901-3199	0.6343
Periclase	Mg O	96-901-3225	0.6268
Bis(oxoniobium) Tetraphosphate(V)	Nb2 O15 P4	96-151-7730	0.6267
	Mo24 O180 P48	96-430-3258	0.6257
Li.19 V O2	Li0.19 O2 V	96-153-0868	0.6111
	Co Ga	96-152-5478	0.6092
Mn3 (Fe (C N)6)2 (H2 O)2	C12 H4 Fe2 Mn3 N12 O2	96-152-6337	0.6016

Search-Match

Settings

Reference database used	COD-Inorg 2021.12.14
Automatic zeropoint adaptation	Yes
Downgrade entries with low scaling factors	Yes
Minimum figure-of-merit (FoM)	0.60
2theta window for peak corr.	0.30 deg.
Minimum rel. int. for peak corr.	0
Parameter/influence 2theta	0.50
Parameter/influence intensities	0.50
Parameter multiple/single phase(s)	0.50

Peak List

No.	*2theta [°]*	*d [Å]*	*I/I0 (peak height)*	*Counts (peak area)*	*FWHM*
1	17.34	5.1100	406.01	611.87	5.9200
2	21.78	4.0773	1000.00	946.98	3.7200
3	44.26	2.0448	272.53	58.28	0.8400
4	64.62	1.4412	298.42	60.77	0.8000
5	77.72	1.2277	387.80	82.92	0.8400

Integrated Profile Areas

Based on calculated profile

Profile area	*Counts*	*Amount*
Overall diffraction profile	370339	100.00%
Background radiation	276727	74.72%
Diffraction peaks	93611	25.28%
Peak area belonging to selected phases	0	0.00%
Unidentified peak area	93611	25.28%

Peak Residuals

Peak data	*Counts*	*Amount*
Overall peak intensity	1761	100.00%
Peak intensity belonging to selected phases	0	0.00%
Unidentified peak intensity	1761	100.00%

Diffraction Pattern Graphics

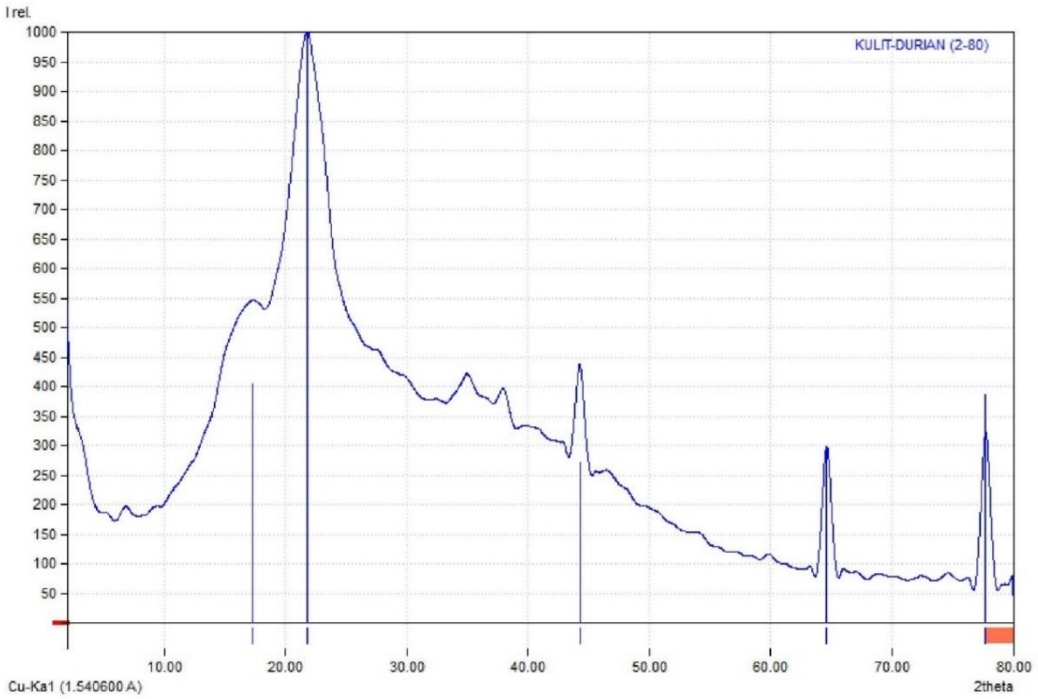

b. Selulosa Kulit Durian

```
////////////////////////////////////////////////////////////
/// Profile Data Ascii Dump (XRD)                        ///
////////////////////////////////////////////////////////////

  Group    : KENSA
  Data     : SELUSOSA_ES
  File Name : SELUSOSA_ES.RAW

# Profile Datafile
       comment          = 2-80
       date & time      = 01-08-22 12:35:28

# Measurement Condition
   X-ray tube
       target          = Cu
       voltage          = 40.0 (kV)
       current          = 30.0 (mA)
   Slits
       divergence slit    = 1.00000 (deg)
       scatter slit      = 1.00000 (deg)
       receiving slit     = 0.15000 (mm)
   Scanning
       drive axis        = Theta-2Theta
       scan range         =   2.000 -  80.000
       scan mode          = Continuous Scan
       scan speed         =   2.0000 (deg/min)
       sampling pitch     =   0.0100 (deg)
       preset time        =   0.30 (sec)
```

c. Aerogel Selulosa

```
/// Profile Data Ascii Dump (XRD)
////////////////////////////////////////////////////////////

  Group    : KENSA
  Data     : Aerogel
  File Name : Aerogel.RAW

# Profile Datafile
       comment          = 2-80
       date & time      = 02-21-22 10:21:43

# Measurement Condition
   X-ray tube
       target          = Cu
       voltage          = 40.0 (kV)
       current          = 30.0 (mA)
   Slits
       divergence slit    = 1.00000 (deg)
       scatter slit      = 1.00000 (deg)
       receiving slit     = 0.15000 (mm)
   Scanning
       drive axis        = Theta-2Theta
       scan range         =   2.000 -  80.000
       scan mode          = Continuous Scan
       scan speed         =   2.0000 (deg/min)
       sampling pitch     =   0.0200 (deg)
       preset time        =   0.60 (sec)
```

Lampiran 19. Hasil Analisis SEM

a) Selulosa Kulit Durian

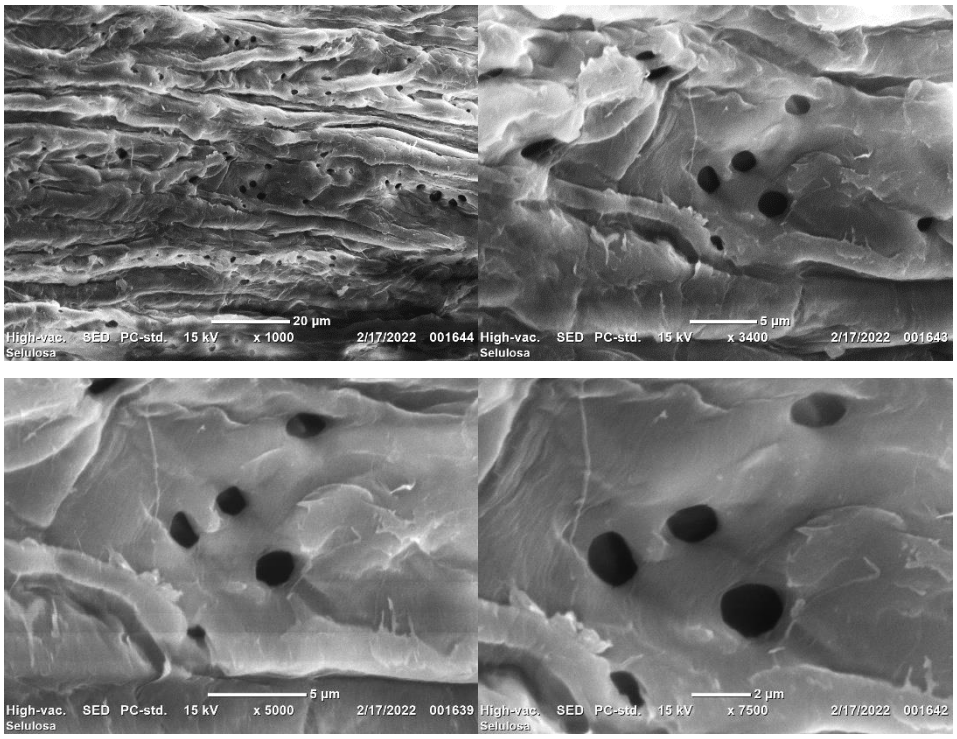

b) Aerogel Selulosa

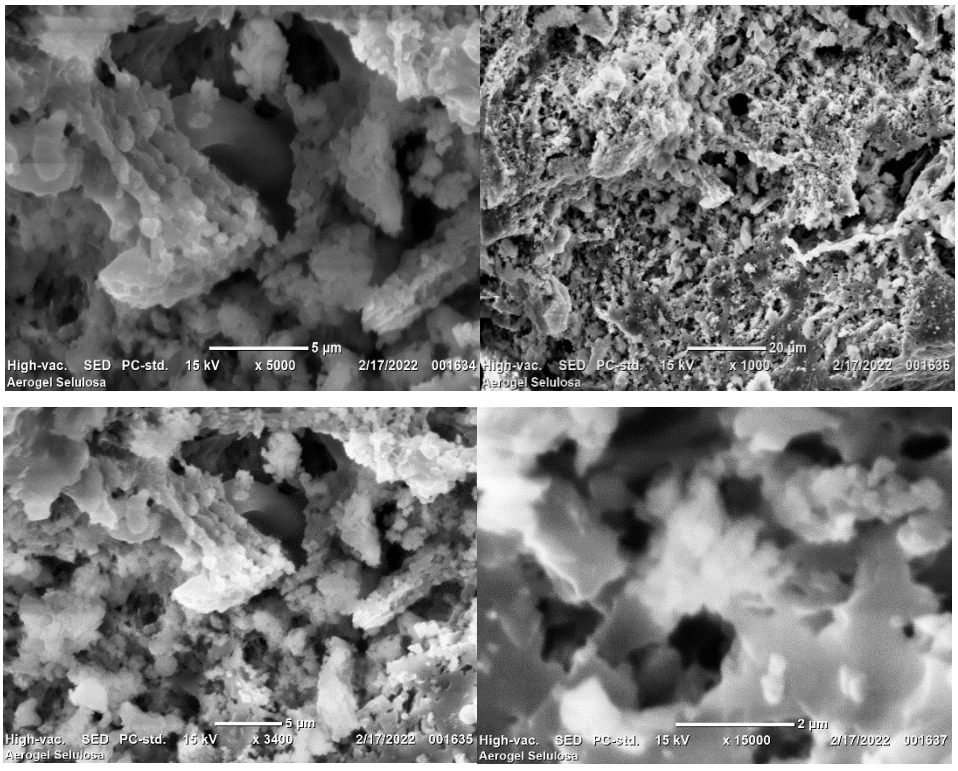

c) Aerogel selulosa setelah mengadsorpsi Cr(VI)

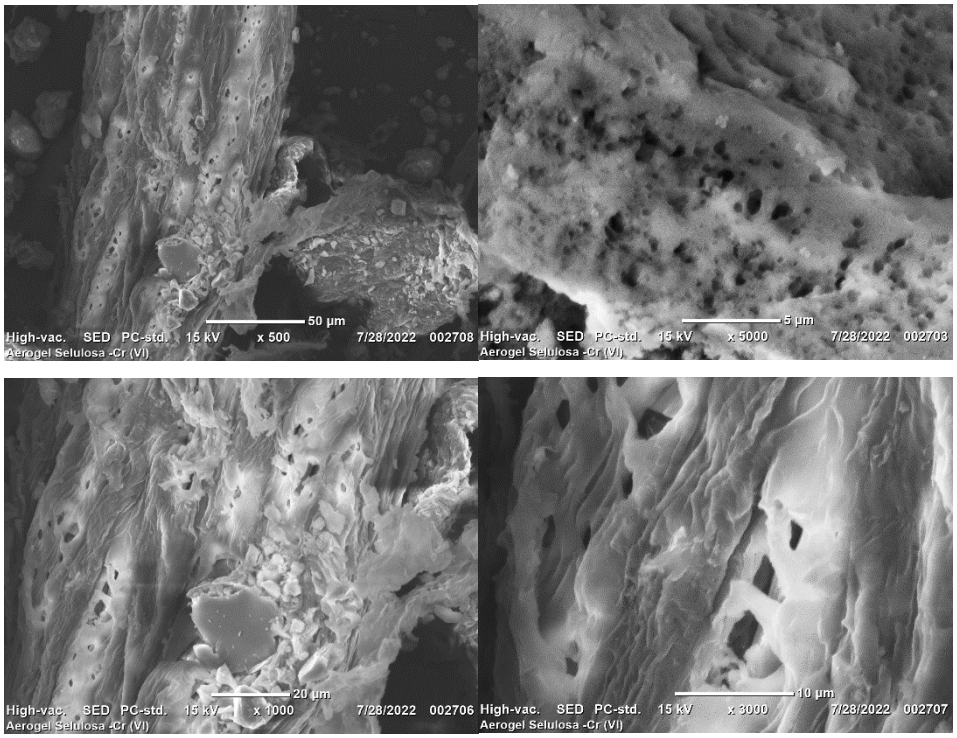

Lampiran 20. Hasil Analisis BET-BJH

micromeritics®

TriStar II 3020 2.00 | TriStar II 3020 Version 2.00 Unit 1 Port 1 | Serial #: 1108 | Page 1

Sample: Aerogel Selulosa
Operator: Sarah
Submitter: 37537
File: C:\TriStar II 3020\data\SAMPEL\2022\...\Aerogel Selulosa.SMP

Started: 4/21/2022 12:50:00 PM
Completed: 4/21/2022 2:11:07 PM
Report Time: 4/22/2022 8:16:19 AM
Sample Mass: 0.6741 g
Cold Free Space: 31.2064 cm³
Low Pressure Dose: None
Automatic Degas: No

Analysis Adsorptive: N2
Analysis Bath Temp.: -195.850 °C
Thermal Correction: No
Warm Free Space: 10.9608 cm³ Measured
Equilibration Interval: 5 s
Sample Density: 1.000 g/cm³

Summary Report

Surface Area

Single point surface area at P/Po = 0.303369944:	2.0610 m²/g
BET Surface Area:	2.1249 m²/g
t-Plot External Surface Area:	2.3914 m²/g
BJH Adsorption cumulative surface area of pores between 1.7000 nm and 300.0000 nm diameter:	2.141 m²/g
BJH Desorption cumulative surface area of pores between 1.7000 nm and 300.0000 nm diameter:	2.2928 m²/g
D-H Adsorption cumulative surface area of pores between 1.7000 nm and 300.0000 nm diameter:	1.884 m²/g
D-H Desorption cumulative surface area of pores between 1.7000 nm and 300.0000 nm diameter:	2.3032 m²/g

Pore Volume

Single point adsorption total pore volume of pores less than 171.9564 nm diameter at P/Po = 0.988729858:	0.010222 cm³/g
t-Plot micropore volume:	-0.000141 cm³/g
BJH Adsorption cumulative volume of pores between 1.7000 nm and 300.0000 nm diameter:	0.010049 cm³/g
BJH Desorption cumulative volume of pores between 1.7000 nm and 300.0000 nm diameter:	0.009939 cm³/g

Pore Size

Adsorption average pore width (4V/A by BET):	19.24200 nm
BJH Adsorption average pore diameter (4V/A):	18.7742 nm
BJH Desorption average pore diameter (4V/A):	17.3402 nm
D-H Adsorption average pore diameter (4V/A):	21.0934 nm
D-H Desorption average pore diameter (4V/A):	17.4359 nm

micromeritics®

Sample: Aerogel Selulosa
Operator: Sarah
Submitter: 37537
File: C:\TriStar II 3020\data\SAMPEL\2022\...\Aerogel Selulosa.SMP

Started:	4/21/2022 12:50:00 PM	Analysis Adsorptive:	N2
Completed:	4/21/2022 2:11:07 PM	Analysis Bath Temp.:	-195.850 °C
Report Time:	4/22/2022 8:16:19 AM	Thermal Correction:	No
Sample Mass:	0.6741 g	Warm Free Space:	10.9608 cm³ Measured
Cold Free Space:	31.2064 cm³	Equilibration Interval:	5 s
Low Pressure Dose:	None	Sample Density:	1.000 g/cm³
Automatic Degas:	No		

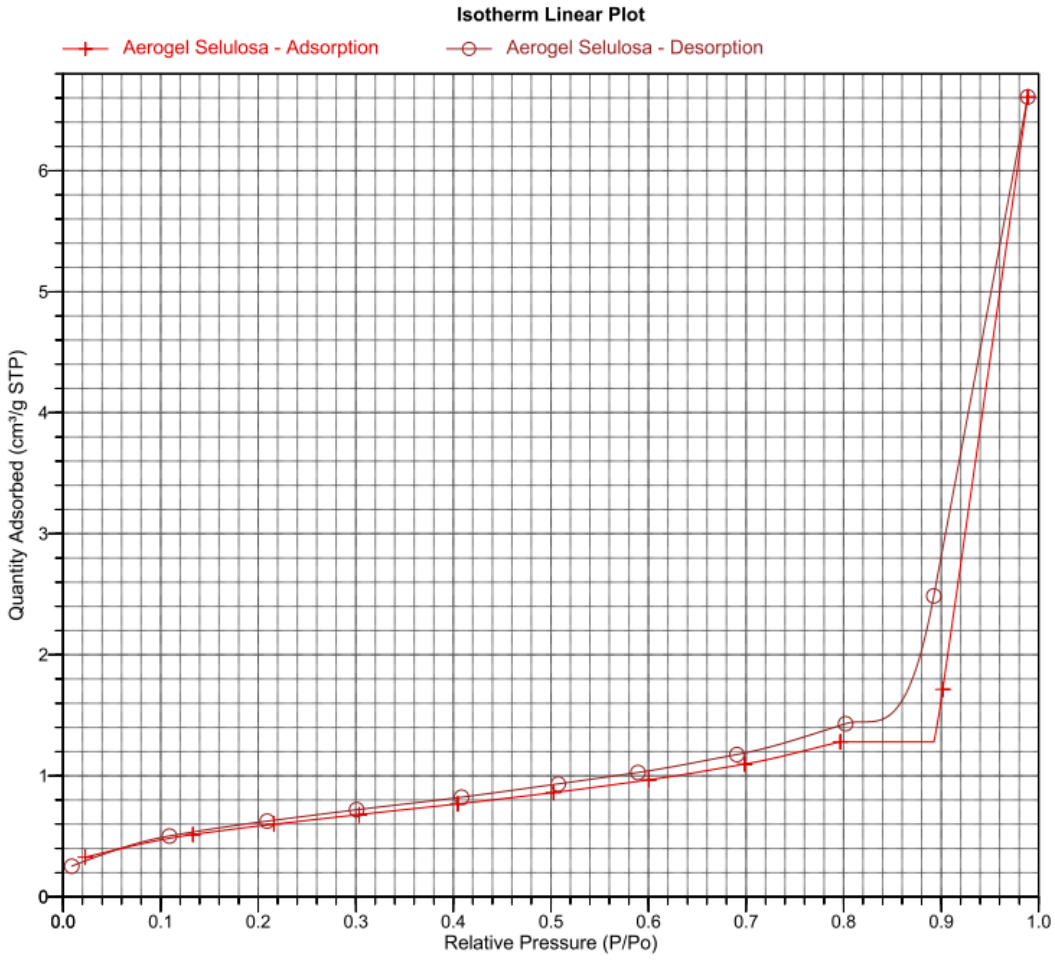

micromeritics®

Sample: Aerogel Selulosa
Operator: Sarah
Submitter: 37537
File: C:\TriStar II 3020\data\SAMPEL\2022\...\Aerogel Selulosa.SMP

Started: 4/21/2022 12:50:00 PM
Completed: 4/21/2022 2:11:07 PM
Report Time: 4/22/2022 8:16:19 AM
Sample Mass: 0.6741 g
Cold Free Space: 31.2064 cm³
Low Pressure Dose: None
Automatic Degas: No

Analysis Adsorptive: N2
Analysis Bath Temp.: -195.850 °C
Thermal Correction: No
Warm Free Space: 10.9608 cm³ Measured
Equilibration Interval: 5 s
Sample Density: 1.000 g/cm³

BJH Adsorption Pore Distribution Report

Faas Correction
Harkins and Jura
t = [13.99 / (0.034 - log(P/Po))] ^ 0.5

Diameter Range: 1.7000 nm to 300.0000 nm
Adsorbate Property Factor: 0.95300 nm
Density Conversion Factor: 0.0015468
Fraction of Pores Open at Both Ends: 0.00

Pore Diameter Range (nm)	Average Diameter (nm)	Incremental Pore Volume (cm³/g)	Cumulative Pore Volume (cm³/g)	Incremental Pore Area (m²/g)	Cumulative Pore Area (m²/g)
171.8 - 20.9	22.8	0.009536	0.009536	1.676	1.676
20.9 - 10.3	12.1	0.000293	0.009829	0.097	1.773
10.3 - 6.9	7.8	0.000016	0.009845	0.008	1.781
6.9 - 5.0	5.6	0.000006	0.009852	0.005	1.786
5.0 - 3.9	4.3	0.000016	0.009867	0.015	1.800
3.9 - 3.1	3.4	0.000029	0.009896	0.034	1.834
3.1 - 2.4	2.7	0.000034	0.009930	0.051	1.885
2.4 - 2.0	2.1	0.000050	0.009980	0.094	1.979
2.0 - 1.5	1.7	0.000069	0.010049	0.162	2.141

micromeritics®

Sample: Aerogel Selulosa
Operator: Sarah
Submitter: 37537
File: C:\TriStar II 3020\data\SAMPEL\2022\...\Aerogel Selulosa.SMP

Started: 4/21/2022 12:50:00 PM
Completed: 4/21/2022 2:11:07 PM
Report Time: 4/22/2022 8:16:19 AM
Sample Mass: 0.6741 g
Cold Free Space: 31.2064 cm³
Low Pressure Dose: None
Automatic Degas: No

Analysis Adsorptive: N2
Analysis Bath Temp.: -195.850 °C
Thermal Correction: No
Warm Free Space: 10.9608 cm³ Measured
Equilibration Interval: 5 s
Sample Density: 1.000 g/cm³

BJH Desorption Pore Distribution Report

Faas Correction
Harkins and Jura
t = [13.99 / (0.034 - log(P/Po))] ^ 0.5

Diameter Range: 1.7000 nm to 300.0000 nm
Adsorbate Property Factor: 0.95300 nm
Density Conversion Factor: 0.0015468
Fraction of Pores Open at Both Ends: 0.00

Pore Diameter Range (nm)	Average Diameter (nm)	Incremental Pore Volume (cm³/g)	Cumulative Pore Volume (cm³/g)	Incremental Pore Area (m²/g)	Cumulative Pore Area (m²/g)
171.7 - 19.1	20.6	0.008079	0.008079	1.567	1.567
19.1 - 10.4	12.3	0.001741	0.009820	0.568	2.135
10.4 - 6.6	7.6	0.000037	0.009857	0.020	2.154
6.6 - 3.0	3.3	0.000022	0.009879	0.027	2.181
3.0 - 2.3	2.6	0.000017	0.009896	0.027	2.208
2.3 - 1.8	2.0	0.000043	0.009939	0.085	2.293